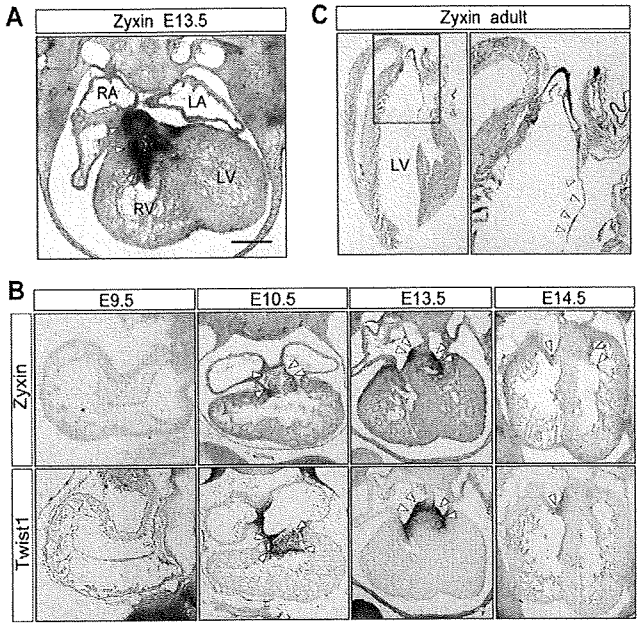

Figure 3. Zyxin is expressed in AVC during cardiac morphogenesis and valves in adult. (A) In situ hybridization for *zyxin* in E13.5 mouse embryo. Arrowheads indicate the strong expression of zyxin in AVC. RA, LA, RV, and LV stand for right atrium, left atrium, right ventricle, and left ventricle, respectively. Scale bar, 250 μm. (B) In situ hybridization for *zyxin* or *Twist1* from E9.5 to E14.5. Arrowheads indicate the expression of each gene. Note that the expression pattern of zyxin and Twist1 are highly correlated with each other. (C) In situ hybridization for *zyxin* in adult heart. The black square indicates the region of higher magnification shown to the right. Arrowhead indicates the zyxin expression in the mitral valve.

of cells (Figure 4D, Migratory), only 22% of the shZyxin-transduced explants exhibited endocardial cell migration and the majority remained cobblestone-like appearance (Figure 4D, Nonmigratory).

Invasiveness into extracellular matrices is an important feature for the endocardial cells that undergo EMT, because it is required for the endocardial cushion cellularization (Niessen *et al.*, 2008). Therefore, we examined the invasiveness of the explanted endocardial cells into collagen gel by confocal microscopy. Consequently, invasion of the zyxin-depleted cells was significantly reduced compared with the control cells (Figure 4E). Finally, the effect of zyxin depletion on actin fiber formation was addressed in the explanted cells. Although the prominent actin stress fiber formation was observed in shLacZ-transduced explants (Figure 4F, LacZ shRNA), only scarce actin network formation was seen in the shZyxin-transduced explants (Figure 4F, zyxin shRNA). These findings suggest that zyxin contributes to the endocardial EMT by regulating cell motility though the reorganization of actin fibers.

Twist1 Regulates Zyxin in TGF-β1-EMT

To clarify how zyxin expression is regulated during EMT, we tested the potential transcription factors that are reported to promote EMT (Thuault *et al.*, 2006). NMuMG-C7 cells expressed Twist1, Twist2, TwistNB, Snail, and HMGA2 (Figure 5A). Among them, the expression of Twist1 and Snail was increased by TGF-β1 treatment (Figure 5A). Subsequently, we transduced NMuMG-C7 cells with retrovirus vectors expressing Snail, Twist1, HMGA2 (Thuault *et al.*, 2006), or control EGFP. Among them, Twist1 up-regulated zyxin mRNA (Figure 5B) and induced zyxin expression (Figure 5C). These results suggest that Twist1 can promote zyxin expression. We then studied the requirement of Twist1 for zyxin up-regulation by TGF-β1. On knockdown of Twist1 (Figure 5D), TGF-β1 failed to up-regulate zyxin mRNA (Figure 5E) and to induce the expression of zyxin (Figure 5, F and G). Twist1 knockdown also decreased the basal expression of zyxin, suggesting the contribution of Twist1 to the basal expression of zyxin (Figure 5, F and G). We then studied whether focal adhesion-related proteins were generally regulated by TGF-β1 or Twist1. We investigated the expression of paxillin, FAK, vinculin, and p130Cas. Among them, paxillin was up-regulated by TGF-β1 (Supplementary Figure S5A). Twist1 depletion by siTwist1, however, did not abrogate the up-regulation of paxillin by TGF-β1 (Supplementary Figure S5B). These results suggest that focal adhesion proteins are not generally regulated by a single transcription factor in TGF-β1–induced EMT. Next, we investigated the possibility that paxillin was regulated by Snail, which was up-regulated by TGF-β1 (Figure 5A). We found paxillin was not up-regulated by Snail, either (Supplementary Figure S5C). These results delineate the signaling pathway, TGF-β1-Twist1-zyxin in the EMT and raise the possibility that different sets of focal adhesion proteins are regulated by distinct transcription factors.

Twist1 Uses Zyxin to Execute EMT

Twist1 is a potent EMT inducer, the function of which is well-characterized in cancer metastasis (Ansieau *et al.*, 2008). We explored whether zyxin is required for Twist1-induced EMT. NMuMG-C7 cells transduced with Twist1 (NMuMG-Twist1) underwent EMT and exhibited cell scattering, numerous protrusions (Figure 6A, arrowhead) and stress fiber formation (Figure 6C). In contrast, NMuMG-Twist1 cells transfected with zyxin siRNA exhibited fewer protrusions and rectangular cell morphology (Figure 6B). Actin stress fiber formation was also attenuated (Figure 6D). These findings suggest that zyxin is required for the cell shape change and actin fiber formation induced by Twist1. In addition, although NMuMG-Twist1 cells displayed enhanced migratory activity, depletion of zyxin strongly suppressed the migration of NMuMG-Twist1 cells (Figure 6, E and F). These results suggest that Twist1 induces EMT by up-regulating zyxin and by potential zyxin-dependent effects on actin reorganization to promote cell migration.

Thus, zyxin plays a significant role in motility acquisition in EMT by promoting actin fiber formation and confers the

Figure 2 (cont). or scramble RNA and treated or not with TGF-β1 for 24 h. Apical and basal actin network were observed separately with a confocal microscope. Note that both the apical and basal actin fiber formation were hampered by zyxin depletion. Scale bar, 50 μm. (L) The scheme of EGFP-tagged zyxin deletion constructs. EGFP–zyxin constructs were introduced into NMuMG-C7 cells by transient transfection. FL: full length. (M) NMuMG-C7 cells were transduced with lentivirus vector that expresses shZyxin that targets 3′UTR. The resultant cells were then transfected with the EGFP–zyxin constructs that lack 3′UTR. The suppression of endogenous zyxin and the expression of transfected genes were confirmed by blotting with anti-zyxin and ant-EGFP antibodies. LIM only construct lacks the epitope recognized by zyxin antibody. (N) Neither ΔLIM nor LIM only constructs rescued the endogenous zyxin depletion. Endogenous zyxin-depleted cells were transfected with EGFP–zyxin constructs and treated with TGF-β1 for 24 h. Actin fiber formation was observed in the cells transfected with FL (arrowhead), but not with ΔLIM or LIM only constructs. Scale bar, 50 μm.

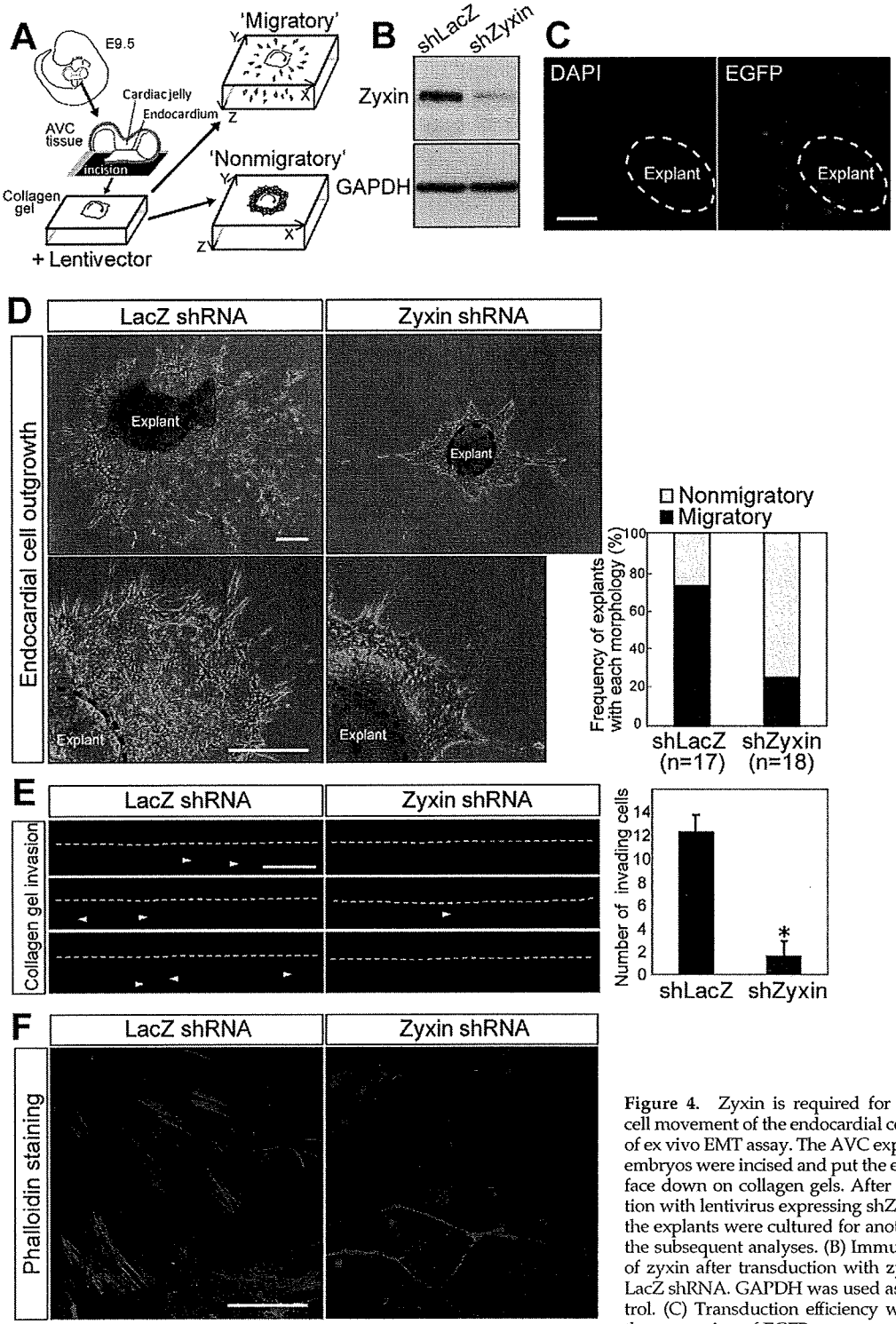

Figure 4. Zyxin is required for morphogenetic cell movement of the endocardial cells. (A) Scheme of ex vivo EMT assay. The AVC explants from E9.5 embryos were incised and put the endocardial surface down on collagen gels. After 24 h of incubation with lentivirus expressing shZyxin or shLacZ, the explants were cultured for another 48 h before the subsequent analyses. (B) Immunoblot analysis of zyxin after transduction with zyxin shRNA or LacZ shRNA. GAPDH was used as a loading control. (C) Transduction efficiency was assessed by the expression of EGFP coexpressed with shRNA. After 48 h of incubation after transduction, the explants were stained with DAPI and subjected to fluorescent microscopy. Scale bar, 100 μm. (D) Depletion of zyxin abolished the outgrowth of the endocardial cells. Phase-contrast images of AVC explants after 48 h of incubation after transduction. Scale bars, 250 μm. Right graph shows the proportion of colonies with the morphology defined by criteria described in *Materials and Methods*. (E) Cell invasiveness was suppressed by zyxin depletion. Collagen gel invasiveness assessed by XZ confocal microscopy. After 48 h of incubation after transduction, the explants were fixed and stained with DAPI. Broken lines indicate the surface of the gel. Scale bar, 100 μm. Right panel shows the number of the cells invading into the gel per unit area presented as mean ± SEM (n = 6). *p = 0.0048 versus shLacZ. (F) Zyxin is required for actin fiber reorganization in the endocardial cells. After 48 h of incubation after transduction, the explants were fixed and stained with phalloidin and DAPI and subjected to confocal microscopy. Note the decreased actin stress fibers in the endocardial cells that underwent EMT upon the collagen gel. Scale bar, 50 μm.

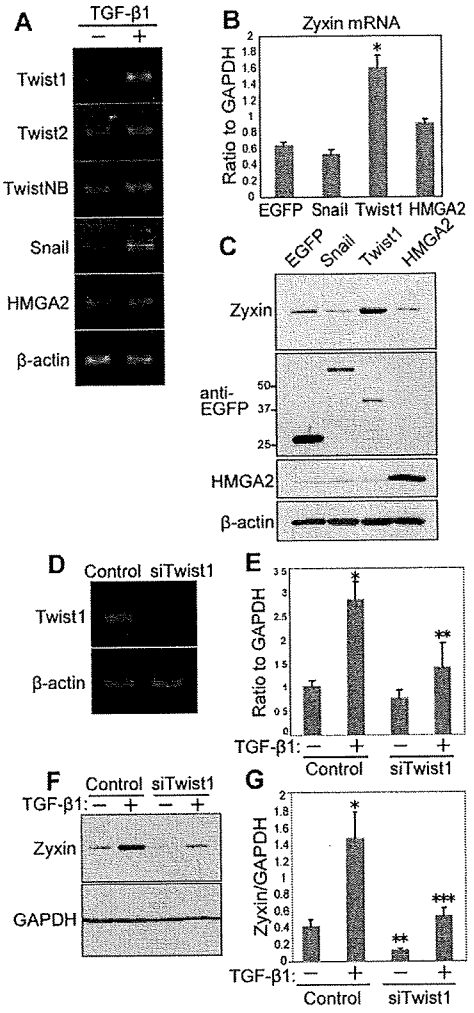

Figure 5. Twist1 regulates zyxin in TGF-β1-EMT. (A) Expression analysis of EMT inducers in NMuMG-C7 cells. RT-PCR performed with total RNA isolated from NMuMG-C7 cells treated with or without TGF-β1. β-Actin was used as a control. (B) Twist1 up-regulates zyxin. Real-time PCR performed with total RNA from NMuMG-C7 cells transduced with EGFP, Snail, Twist1, or HMGA2. *p = 0.0122 versus EGFP. Error bars, the SEM of three technical replicates. (C) Twist1 induced the expression of zyxin. Immunoblot analysis of zyxin in NMuMG-C7 cells transduced with EGFP, EGFP-Snail, EGFP-Twist1, or HMGA2. The expression of transduced genes was confirmed by blotting with anti-EGFP and anti-HMGA2 antibodies. (D) Efficacy of Twist1 RNAi assessed by RT-PCR. Total RNA from NMuMG-C7 cells transfected with either Twist1 siRNA or scramble RNA were subjected to RT-PCR. (E) Twist1 depletion abrogated up-regulation of zyxin by TGF-β1. Real-time PCR analysis of zyxin mRNA in NMuMG-C7 cells transfected with Twist1 siRNA or scramble RNA and treated or not with TGF-β1. Results are shown as the mean ± SEM (n = 3). *p = 0.011 when compared with control, TGF-β1(−); **p = 0.0236 when compared with control, TGF-β1(+). (F) Twist1 depletion suppressed the expression of zyxin. Immunoblot analysis of zyxin in NMuMG-C7 cells transfected with Twist1 siRNA or scramble RNA and treated or not with TGF-β1. GAPDH was used as a loading control. (G) Results of F were quantitated by densitometry using NIH ImageJ. Error bars, SD from triplicate experiments. *p = 0.0084 when compared with control, TGF-β1(−); **p = 0.035 when compared with control, TGF-β1(−); ***p = 0.012 when compared with control, TGF-β1(+).

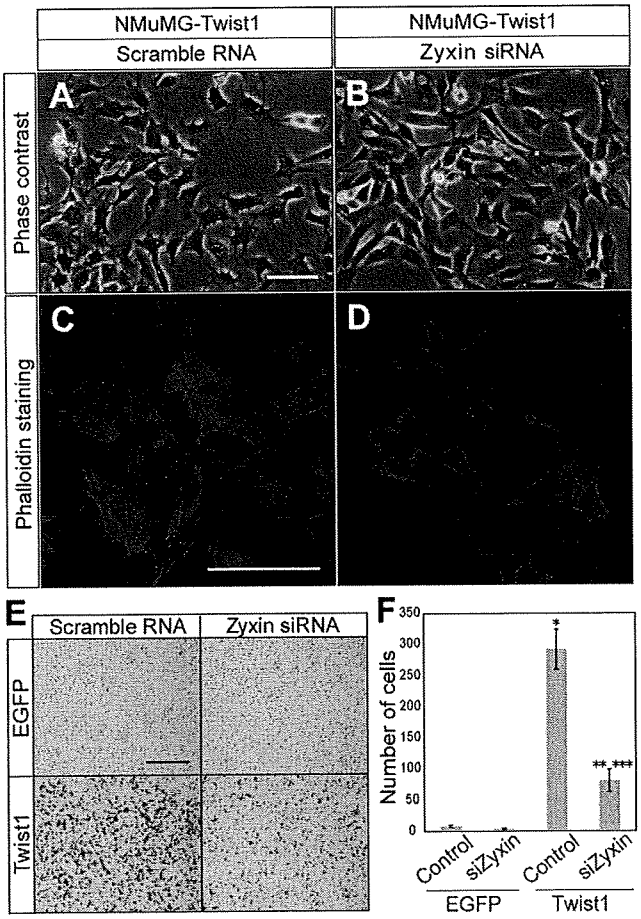

Figure 6. Twist1 uses zyxin to execute EMT. (A and B) Twist1-induced cell morphological change was abrogated by zyxin depletion. NMuMG-C7 cells transduced with Twist1 were transfected with zyxin siRNA or scramble RNA. Phase-contrast microscopy was done 48 h after transfection. (A) Arrowheads indicate the cell protrusions induced by Twist1 transduction. Scale bar, 100 μm. (C and D) Twist1-induced actin fiber reorganization was abrogated by zyxin depletion. Phalloidin staining in NMuMG-Twist1 cells transfected with zyxin siRNA or scramble RNA. Scale bar, 100 μm. (E) Modified Boyden's chamber assay performed with NMuMG-Twist1 cells transfected with zyxin siRNA or scramble RNA. After incubation for 4 h, the cells that migrated to the lower surface of the membrane were stained. Scale bar, 250 μm. (F) The number of migrated cells in E. *p = 0.0013 versus NMuMG-EGFP, Control; **p = 0.0144 versus NMuMG-Twist1, Control; ***p = 0.0184 versus NMuMG-EGFP, Control. Results are shown as the mean ± SEM of four separate migration assays from two independent experiments.

endocardial cells the motility required for cardiac morphogenesis.

DISCUSSION

We delineate the signaling pathway, TGF-β1-Twist1-zyxin, in the EMT in cultured cells and demonstrate the involvement of this signaling in valvulogenesis in the development of the heart in vivo. Depletion of zyxin abrogated either Twist1-dependent or TGF-β1–dependent EMT in NMuMG cells, confirming this signaling.

We show that zyxin is essential for cell migration and actin fiber reorganization in TGF-β1-EMT. Zyxin and paxil-

lin are the prototypes of two related subfamilies of LIM domain proteins that are localized primarily at focal adhesion plaques (Wang and Gilmore, 2003). Although paxillin and Hic-5 are required for the progression of EMT (Tumbarello *et al.*, 2005), the involvement of zyxin in EMT has not been reported. On EMT induction, zyxin mobilized from focal adhesions to actin stress fibers. Although our findings are based on EGFP-fusion protein study, EGFP-tagged zyxin was reported to display a distribution pattern that is indistinguishable from that of the endogenous zyxin (Nix *et al.*, 2001; Hotulainen and Lappalainen, 2006). Mechanostress-induced relocation of zyxin has been reported (Yoshigi *et al.*, 2005). Yoshigi *et al.* showed that cyclic stretch or sheer stress to cells in vitro resulted in mobilization of zyxin from focal adhesions to actin filaments. Lele *et al.* (2006) measured the molecular binding kinetics of focal adhesion proteins in living cells using modified fluorescence recovery after photobleaching technique and showed mechanical forces specifically altered the molecular binding kinetics of zyxin, but not of vinculin. What role does the relocation of zyxin play, if any, in endocardial morphogenesis? Yashiro *et al.* (2007) has shown that left-right asymmetry of aortic arch was determined by asymmetric blood flow during the development of great arteries. Similarly, sheer stress induced by blood flow or mechanostress altered through cardiac morphogenesis might induce the relocation of proteins that sense mechanical forces, thereby contributing to endocardial morphogenesis. The significance of relocation requires further analysis, although it is speculated that zyxin interacts with a set of proteins such as VASP (Yoshigi *et al.*, 2005) as an adaptor protein on the actin stress fibers. The cells transfected with zyxin siRNA failed to show TGF-β1–enhanced cell motility and fiber formation, indicating that zyxin is essential for motility acquisition and actin fiber reorganization induced by TGF-β1 in NMuMG cells.

We delineated the signaling pathway, TGF-β1-Twist1-zyxin in EMT. TGF-β1 induced the expression of Twist1 and Snail. Twist1, but not Snail, was required for the up-regulation of zyxin by TGF-β1. Numerous focal adhesion proteins are regulated in EMT (Zavadil and Bottinger, 2005). In NMuMG-C7 cells, paxillin was up-regulated by TGF-β1 (Supplementary Figure S5A), but neither Twist1 nor Snail induced paxillin expression, suggesting the other transcription factor was responsible for it. It is of note that Twist1 or Snail targets different genes despite that both are potent EMT inducers. These results implied the multiple layers of transcriptional regulation in EMT. Coordinated expression of transcription factors might be important for the efficient progression of EMT. Niessen *et al.* showed that Snail and Slug, which belong to the same protein family, are regulated differentially and function in combination during AVC morphogenesis (Niessen *et al.*, 2008). Thuault *et al.* (2006) showed that HMGA2 induces the expression of Snail/Slug and weakly of Twist1 in TGF-β1–induced EMT. These reports support that EMT is more efficiently executed by coordination of multiple transcriptional regulations. Further investigation is necessary to address how the cellular phenomena are regulated by multiple layers of transcriptional regulation.

Twist1 is an EMT regulator well characterized in cancer metastasis (Yang *et al.*, 2004). It is of note that Twist1 uses zyxin to induce the cell morphological change and migration. Therefore, zyxin might be a target of treatment or prevention for cancer metastasis. We confirmed the presence of several E-box sites, which basic helix-loop-helix transcription factors including Twist1 preferentially bind to, in the promoter region of zyxin gene. Further analysis is needed to reveal how Twist1 promotes transcription of zyxin.

We revealed that zyxin was predominantly expressed in AVC in the embryonic heart undergoing EMT and that zyxin was required for migration and actin fiber reorganization in the endocardial cells. The expression of zyxin mRNA began at E10.5 that corresponds to the onset of endocardial EMT and became predominant in AVC of developing heart and in adult valves. The expression of Twist1 in AVC was highly correlated with that of zyxin. TGF-β1 is expressed in AVC and contributes to valvulogenesis (Nakajima *et al.*, 2000; Molin *et al.*, 2003), suggesting functional coordination of TGF-β1-Twist1-zyxin pathway in vivo. Most recently, the role for Twist1 in AVC development was reported (Shelton and Yutzey, 2008), and further molecular dissection would lead to better understanding of cardiac morphogenesis.

We further examined the importance of zyxin in EMT by ex vivo assay using E9.5 AVC tissue explants. The endocardial cells transduced with lentivirus vector expressing zyxin shRNA failed to exhibit outgrowth and invasiveness into collagen gels and to execute actin fiber reorganization. Together, zyxin is essential for the endocardial cells to undergo EMT in which zyxin promotes cell migration through actin fiber reorganization. Although zyxin-null mice are viable and fertile (Hoffman *et al.*, 2003), the hearts of the zyxin-null mice have not been inspected in detail. We considered two possibilities for no phenotype in zyxin-null mice. First, the abnormalities might be minor ones requiring careful observation, such as bicuspid aortic valves (Garg *et al.*, 2005) or malformation of supporting apparatus such as chordae tendineae (Norris *et al.*, 2008). Second, there might be genetic redundancy and chronic loss of zyxin might be overcome. To support this, although single knockout mice of VASP, with which zyxin directly interacts, exhibit no cardiac phenotype, but triple knockout mice of VASP, Ena and Ena-VASP-like show abnormally thin endocardium (Furman *et al.*, 2007). It might be necessary to ablate plural genes including LIM-family proteins to observe abnormal phenotypes due to the absence of zyxin. In *Xenopus laevis*, Martynova *et al.* (2008) revealed that zyxin expression increased along gastrulation that is another example of developmental EMT, and administration of zyxin morpholino resulted in disruption of embryos during gastrulation. It implied the essential role for zyxin in EMT during gastrulation. Thus, considering the particularly strong expression of zyxin in AVC undergoing EMT and the result from ex vivo AVC explant assay, we conclude that zyxin is required for migration and actin fiber reorganization of the endocardial cells.

In this study, we delineate the essential signaling, TGF-β1-Twist1-zyxin pathway, in in vitro EMT using cultured cells and in vivo EMT using the developing heart.

ACKNOWLEDGMENTS

We thank Tsuyoshi Akagi for providing pCX4 vectors. This work was supported by grants from the Ministry of Education, Culture, Sports, Science and Technology, Japan Heart Association, and Miyata Heart Foundation.

REFERENCES

Akagi, T., Sasai, K., and Hanafusa, H. (2003). Refractory nature of normal human diploid fibroblasts with respect to oncogene-mediated transformation. Proc. Natl. Acad. Sci. USA. *100*, 13567–13572.

Ansieau, S., *et al.* (2008). Induction of EMT by twist proteins as a collateral effect of tumor-promoting inactivation of premature senescence. Cancer Cell *14*, 79–89.

Bartram, U., Molin, D. G., Wisse, L. J., Mohamad, A., Sanford, L. P., Doetschman, T., Speer, C. P., Poelmann, R. E., and Gittenberger-de Groot, A. C. (2001). Double-outlet right ventricle and overriding tricuspid valve reflect disturbances of looping, myocardialization, endocardial cushion differentiation, and apoptosis in TGF-beta(2)-knockout mice. Circulation *103*, 2745–2752.

Beckerle, M. C. (1998). Spatial control of actin filament assembly: lessons from *Listeria*. Cell *95*, 741–748.

Bruneau, B. G. (2008). The developmental genetics of congenital heart disease. Nature *451*, 943–948.

Camenisch, T. D., Molin, D. G., Person, A., Runyan, R. B., Gittenberger-de Groot, A. C., McDonald, J. A., and Klewer, S. E. (2002). Temporal and distinct TGFbeta ligand requirements during mouse and avian endocardial cushion morphogenesis. Dev. Biol. *248*, 170–181.

Cano, A., Perez-Moreno, M. A., Rodrigo, I., Locascio, A., Blanco, M. J., del Barrio, M. G., Portillo, F., and Nieto, M. A. (2000). The transcription factor snail controls epithelial-mesenchymal transitions by repressing E-cadherin expression. Nat. Cell Biol. *2*, 76–83.

Chang, C. P., Neilson, J. R., Bayle, J. H., Gestwicki, J. E., Kuo, A., Stankunas, K., Graef, I. A., and Crabtree, G. R. (2004). A field of myocardial-endocardial NFAT signaling underlies heart valve morphogenesis. Cell *118*, 649–663.

Fradelizi, J., Noireaux, V., Plastino, J., Menichi, B., Louvard, D., Sykes, C., Golsteyn, R. M., and Friederich, E. (2001). ActA and human zyxin harbour Arp2/3-independent actin-polymerization activity. Nat. Cell Biol. *3*, 699–707.

Furman, C., Sieminski, A. L., Kwiatkowski, A. V., Rubinson, D. A., Vasile, E., Bronson, R. T., Fassler, R., and Gertler, F. B. (2007). Ena/VASP is required for endothelial barrier function in vivo. J. Cell Biol. *179*, 761–775.

Garg, V., Muth, A. N., Ransom, J. F., Schluterman, M. K., Barnes, R., King, I. N., Grossfeld, P. D., and Srivastava, D. (2005). Mutations in NOTCH1 cause aortic valve disease. Nature *437*, 270–274.

Hayashi, M., Nimura, K., Kashiwagi, K., Harada, T., Takaoka, K., Kato, H., Tamai, K., and Kaneda, Y. (2007). Comparative roles of Twist-1 and Id1 in transcriptional regulation by BMP signaling. J. Cell Sci. *120*, 1350–1357.

Hetey, S. E., Lalonde, D. P., and Turner, C. E. (2005). Tyrosine-phosphorylated Hic-5 inhibits epidermal growth factor-induced lamellipodia formation. Exp. Cell Res. *311*, 147–156.

Hoffman, L. M., *et al.* (2003). Targeted disruption of the murine zyxin gene. Mol. Cell Biol. *23*, 70–79.

Hotulainen, P., and Lappalainen, P. (2006). Stress fibers are generated by two distinct actin assembly mechanisms in motile cells. J. Cell Biol. *173*, 383–394.

Kadrmas, J. L., and Beckerle, M. C. (2004). The LIM domain: from the cytoskeleton to the nucleus. Nat. Rev. Mol. Cell Biol. *5*, 920–931.

Koibuchi, N., and Chin, M. T. (2007). CHF1/Hey2 plays a pivotal role in left ventricular maturation through suppression of ectopic atrial gene expression. Circ. Res. *100*, 850–855.

Lele, T. P., Pendse, J., Kumar, S., Salanga, M., Karavitis, J., and Ingber, D. E. (2006). Mechanical forces alter zyxin unbinding kinetics within focal adhesions of living cells. J. Cell Physiol. *207*, 187–194.

Lowry, O. H., Rosebrough, N. J., Farr, A. L., and Randall, R. J. (1951). Protein measurement with the Folin phenol reagent. J. Biol. Chem. *193*, 265–275.

Ma, L., Lu, M. F., Schwartz, R. J., and Martin, J. F. (2005). Bmp2 is essential for cardiac cushion epithelial-mesenchymal transition and myocardial patterning. Development *132*, 5601–5611.

Martynova, N. Y., Eroshkin, F. M., Ermolina, L. V., Ermakova, G. V., Korotaeva, A. L., Smurova, K. M., Gyoeva, F. K., and Zaraisky, A. G. (2008). The LIM-domain protein zyxin binds the homeodomain factor Xanf1/Hesx1 and modulates its activity in the anterior neural plate of *Xenopus laevis* embryo. Dev. Dyn. *237*, 736–749.

Miettinen, P. J., Ebner, R., Lopez, A. R., and Derynck, R. (1994). TGF-beta induced transdifferentiation of mammary epithelial cells to mesenchymal cells: involvement of type I receptors. J. Cell Biol. *127*, 2021–2036.

Molin, D. G., Bartram, U., Van der Heiden, K., Van Iperen, L., Speer, C. P., Hierck, B. P., Poelmann, R. E., and Gittenberger-de-Groot, A. C. (2003). Expression patterns of Tgfbeta1–3 associate with myocardialisation of the outflow tract and the development of the epicardium and the fibrous heart skeleton. Dev. Dyn. *227*, 431–444.

Nakajima, Y., Yamagishi, T., Hokari, S., and Nakamura, H. (2000). Mechanisms involved in valvuloseptal endocardial cushion formation in early cardiogenesis: roles of transforming growth factor (TGF)-beta and bone morphogenetic protein (BMP). Anat. Rec. *258*, 119–127.

Nakaya, Y., Sukowati, E. W., Wu, Y., and Sheng, G. (2008). RhoA and microtubule dynamics control cell-basement membrane interaction in EMT during gastrulation. Nat. Cell Biol. *10*, 765–775.

Niessen, K., Fu, Y., Chang, L., Hoodless, P. A., McFadden, D., and Karsan, A. (2008). Slug is a direct Notch target required for initiation of cardiac cushion cellularization. J. Cell Biol. *182*, 315–325.

Nix, D. A., Fradelizi, J., Bockholt, S., Menichi, B., Louvard, D., Friederich, E., and Beckerle, M. C. (2001). Targeting of zyxin to sites of actin membrane interaction and to the nucleus. J. Biol. Chem. *276*, 34759–34767.

Norris, R. A., Moreno-Rodriguez, R. A., Sugi, Y., Hoffman, S., Amos, J., Hart, M. M., Potts, J. D., Goodwin, R. L., and Markwald, R. R. (2008). Periostin regulates atrioventricular valve maturation. Dev. Biol. *316*, 200–213.

Perez-Moreno, M., Jamora, C., and Fuchs, E. (2003). Sticky business: orchestrating cellular signals at adherens junctions. Cell *112*, 535–548.

Runyan, R. B., and Markwald, R. R. (1983). Invasion of mesenchyme into three-dimensional collagen gels: a regional and temporal analysis of interaction in embryonic heart tissue. Dev. Biol. *95*, 108–114.

Saito, Y., *et al.* (2006). Transfection of human hepatocyte growth factor gene ameliorates secondary lymphedema via promotion of lymphangiogenesis. Circulation *114*, 1177–1184.

Sanford, L. P., Ormsby, I., Gittenberger-de Groot, A. C., Sariola, H., Friedman, R., Boivin, G. P., Cardell, E. L., and Doetschman, T. (1997). TGFbeta2 knockout mice have multiple developmental defects that are non-overlapping with other TGFbeta knockout phenotypes. Development *124*, 2659–2670.

Schneichel, K. L., and Beckerle, M. C. (1994). The LIM domain is a modular protein-binding interface. Cell *79*, 211–219.

Shelton, E. L., and Yutzey, K. E. (2008). Twist1 function in endocardial cushion cell proliferation, migration, and differentiation during heart valve development. Dev. Biol. *317*, 282–295.

Sridurongrit, S., Larsson, J., Schwartz, R., Ruiz-Lozano, P., and Kaartinen, V. (2008). Signaling via the Tgf-beta type I receptor Alk5 in heart development. Dev. Biol. *322*, 208–218.

Sung, S. Y., Hsieh, C. L., Wu, D., Chung, L. W., and Johnstone, P. A. (2007). Tumor microenvironment promotes cancer progression, metastasis, and therapeutic resistance. Curr. Probl. Cancer *31*, 36–100.

Thiery, J. P. (2003). Epithelial-mesenchymal transitions in development and pathologies. Curr. Opin. Cell Biol. *15*, 740–746.

Thuault, S., Valcourt, U., Petersen, M., Manfioletti, G., Heldin, C. H., and Moustakas, A. (2006). Transforming growth factor-beta employs HMGA2 to elicit epithelial-mesenchymal transition. J. Cell Biol. *174*, 175–183.

Tumbarello, D. A., Brown, M. C., Hetey, S. E., and Turner, C. E. (2005). Regulation of paxillin family members during epithelial-mesenchymal transformation: a putative role for paxillin delta. J. Cell Sci. *118*, 4849–4863.

Vasioukhin, V., Bauer, C., Yin, M., and Fuchs, E. (2000). Directed actin polymerization is the driving force for epithelial cell-cell adhesion. Cell *100*, 209–219.

Wang, Y., and Gilmore, T. D. (2003). Zyxin and paxillin proteins: focal adhesion plaque LIM domain proteins go nuclear. Biochim. Biophys. Acta *1593*, 115–120.

Yang, J., *et al.* (2004). Twist, a master regulator of morphogenesis, plays an essential role in tumor metastasis. Cell *117*, 927–939.

Yashiro, K., Shiratori, H., and Hamada, H. (2007). Haemodynamics determined by a genetic programme govern asymmetric development of the aortic arch. Nature *450*, 285–288.

Yonemura, S., Itoh, M., Nagafuchi, A., and Tsukita, S. (1995). Cell-to-cell adherens junction formation and actin filament organization: similarities and differences between non-polarized fibroblasts and polarized epithelial cells. J. Cell Sci. *108*(Pt 1), 127–142.

Yoshigi, M., Hoffman, L. M., Jensen, C. C., Yost, H. J., and Beckerle, M. C. (2005). Mechanical force mobilizes zyxin from focal adhesions to actin filaments and regulates cytoskeletal reinforcement. J. Cell Biol. *171*, 209–215.

Zavadil, J., and Bottinger, E. P. (2005). TGF-beta and epithelial-to-mesenchymal transitions. Oncogene *24*, 5764–5774.

Molecular Biology of the Cell
Vol. 20, 1949–1959, April 1, 2009

EphA2 Engages Git1 to Suppress Arf6 Activity Modulating Epithelial Cell–Cell Contacts

Koichi Miura,*† Jin-Min Nam,*‡ Chie Kojima,*‡ Naoki Mochizuki,† and Hisataka Sabe*‡

*Department of Molecular Biology, Osaka Bioscience Institute, Suita, Osaka 565-0874, Japan; ‡Graduate School of Biostudies, Kyoto University, Kyoto 606-8502, Japan; and †Department of Structural Analysis, National Cardiovascular Center Research Institute, Suita, Osaka 565-8565, Japan

Submitted June 2, 2008; Revised January 23, 2009; Accepted January 27, 2009
Monitoring Editor: J. Silvio Gutkind

ADP-ribosylation factor (Arf) 6 activity is crucially involved in the regulation of E-cadherin–based cell–cell adhesions. Erythropoietin-producing hepatocellular carcinoma (Eph)-family receptors recognize ligands, namely, ephrins, anchored to the membrane of apposing cells, and they mediate cell–cell contact-dependent events. Here, we found that Arf6 activity is down-regulated in Madin-Darby canine kidney cells, which is dependent on cell density and calcium ion concentration, and we provide evidence of a novel signaling pathway by which ligand-activated EphA2 suppresses Arf6 activity. This EphA2-mediated suppression of Arf6 activity was linked to the induction of cell compaction and polarization, but it was independent of the down-regulation of extracellular signal-regulated kinase 1/2 kinase activity. We show that G protein-coupled receptor kinase-interacting protein (Git) 1 and noncatalytic region of tyrosine kinase (Nck) 1 are involved in this pathway, in which ligand-activated EphA2, via its phosphorylated Tyr594, binds to the Src homology 2 domain of Nck1, and then via its Src homology 3 domain binds to the synaptic localizing domain of Git1 to suppress Arf6 activity. We propose a positive feedback loop in which E-cadherin–based cell–cell contacts enhance EphA-ephrinA signaling, which in turn down-regulates Arf6 activity to enhance E-cadherin–based cell–cell contacts as well as the apical-basal polarization of epithelial cells.

INTRODUCTION

E-cadherin–mediated cell–cell adhesion is essential for the integrity of epithelial cell layers, as well as their normal functions (Takeichi, 1991; Gumbiner, 2005). ADP-ribosylation factor (Arf) 6 primarily regulates recycling of plasma membrane components, as well as remodeling of the membrane and actin cytoskeleton at the cell peripheries via its GTPase cycle (Donaldson, 2003). It has been shown that expression of an inactive form of Arf6, Arf6T27N, blocks hepatocyte growth factor (HGF)-induced internalization of E-cadherin–based junctional components in Madin-Darby canine kidney (MDCK) epithelial cells, whereas expression of a constitutively active form of Arf6, Arf6Q67L, causes disassembly of adherens junctions (Palacios *et al.*, 2001, 2002). The results of small interfering RNA (siRNA)-mediated knockdown of GEP100, a guanine nucleotide exchanging factor for Arf6, also support a similar notion that inactivation of Arf6 renders resistance to HGF-induced disruption of adherens junctions of human epidermoid carcinoma CaSki cells (Hiroi *et al.*, 2006). Experiments using fetal hepatocyte cells prepared from *Arf6−/−* mice also support this notion (Suzuki *et al.*, 2006). Moreover, we have shown that activation of Arf6 by GEP100 plays a pivotal role in the invasive phenotypes of different breast cancer cells, which is accompanied by the disruption of E-cadherin–mediated cell–cell adhesion in breast cancer MCF7 cells (Morishige *et al.*, 2008). Therefore, down-regulation of Arf6 activity seems to be pivotal for the formation and maintenance of E-cadherin–mediated cell–cell adhesions. However, the mechanism by which Arf6 activity is suppressed in cell–cell contacts has not yet been identified.

Eph receptor tyrosine kinases are classified into either EphA or EphB subfamilies based on the identity of their ligands, ephrinA- and ephrinB-subfamily members, respectively, and both are anchored to the cell membrane by different mechanisms (Pasquale, 2005). Eph receptors and ephrins each have overlapping specificity: several receptors can bind to one ligand, and, in turn, several ligands can bind to one receptor (Pasquale, 2005). The physiological roles of Eph–ephrin interactions have been well characterized in the nervous system, such as during axon guidance and synapse formation, and also in somite and vascular development (Pasquale, 2005). Eph receptors, when ligand-activated, become tyrosine phosphorylated and evoke a variety of different intracellular signaling cascades, which mostly exert negative regulatory effects, such as on migration and proliferative signaling (Miao *et al.*, 2000, 2001, 2003; Noren *et al.*, 2006).

EphA2 is normally expressed at high levels in adult epithelial cells, as well as in restricted regions of the embryo

This article was published online ahead of print in *MBC in Press* (http://www.molbiolcell.org/cgi/doi/10.1091/mbc.E08-06-0549) on February 4, 2009.

Address correspondence to: Hisataka Sabe (sabe@obi.or.jp).

Abbreviations used: Arf, ADP-ribosylation factor; Eph, erythropoietin-producing hepatocellular carcinoma; GAP, GTPase-activating protein; Git, G protein-coupled receptor kinase-interacting protein; GGA, Golgi-localizing, gamma-adaptin ear domain homology, ARF-binding protein; HGF, hepatocyte growth factor; MDCK, Madin-Darby canine kidney; Nck, noncatalytic region of tyrosine kinase; SLD, synaptic localizing domain.

during early development (Ruiz and Robertson, 1994; Surawska *et al.*, 2004). EphA2 is frequently overexpressed in different types of human carcinomas, including those of the breast, lung, prostate, esophagus, and kidney (Surawska *et al.*, 2004). The *EphA2* gene is a direct transcription target of the Ras/Raf/mitogen-activated protein kinase kinase (Mek)/extracellular signal-regulated kinase (Erk)1/2 pathway (Macrae *et al.*, 2005). Overexpression of EphA2 in some carcinomas may hence merely be a result of the activation of this pathway in carcinomas rather than an etiologic event (Macrae *et al.*, 2005). In contrast, it has been demonstrated that stimulation of overexpressed EphA2 in some tumor cells by high concentrations of exogenous ligands can negatively regulate the growth, survival, migration, and invasion of these cells (Zelinski *et al.*, 2001; Noblitt *et al.*, 2004). Moreover, disruption of the *EphA2* gene in mice leads to increased susceptibility to skin carcinogenesis (Guo *et al.*, 2006), suggesting a tumor suppressing role of EphA2.

Here, we found that EphA2, when ligand activated, suppresses Arf6 activity. We show that EphA2 uses G protein-coupled receptor kinase-interacting protein (Git) 1 to suppress Arf6 activities. We describe the precise mechanism by which EphA2 is linked to Git1, and we demonstrate that this pathway acts to enhance E-cadherin–based cell–cell adhesions and the apical-basal polarization of epithelial cells.

MATERIALS AND METHODS

Cells

MDCK cells, obtained from Sh. Tsukita (Kyoto University), and human embryonic kidney (HEK) 293T cells were cultured as described previously (Mazaki *et al.*, 2001). Fetal calf serum was purchased from HyClone Laboratories (Logan, UT).

For the culture of MDCK cells under the "sparse density" and the "dense density," 1×10^6 and 5×10^6 cells, respectively, were seeded onto a Φ 90-mm plastic dish and cultured for a further 24 h before subjecting to analysis.

For ephrinA1 stimulation, cells were treated with nonclustered ephrinA1-Fc (R&D Systems, Minneapolis, MN) at 125 ng/ml or control Fc (R&D Systems) at 62.5 ng/ml for 30 min, unless otherwise indicated.

Antibodies and Chemicals

The rabbit polyclonal antibody against Git2 was generated as described previously (Mazaki *et al.*, 2001). Other antibodies were purchased from commercial sources: rat monoclonal antibodies against E-cadherin (clone ECCD-2, Takara, Kyoto, Japan; and clone DECMA-1, Sigma-Aldrich, St. Louis, MO); rabbit polyclonal antibody against Git1 (H-170; Santa Cruz Biotechnology, Santa Cruz, CA); EphA2 (C-20; Santa Cruz Biotechnology); zona occludens (ZO)-1 (Zymed Laboratories, South San Francisco, CA); Erk1/2 (Cell Signaling Technology, Danvers, MA); FLAG (Sigma-Aldrich); mouse monoclonal antibody (mAb) against Arf6 (3A-1; Santa Cruz Biotechnology); noncatalytic region of tyrosine kinase (Nck) (BD Biosciences, San Jose, CA); Ezrin (EZ-1; Biodesign International, Kennebunk, ME); phospho-Erk1/2 (Cell Signaling Technology), hemagglutinin (HA) (16B12; BAbCo, Richmond, CA); glutathione transferase (GST) (Millipore, Billerica, MA); FLAG (M2; Sigma-Aldrich); nonspecific rabbit and mouse immunoglobulin G (IgG) (Sigma-Aldrich); horseradish peroxidase-conjugated goat anti-rabbit or anti-mouse IgG; $F(ab')_2$ fragments of biotin-conjugated goat anti-rabbit or anti-mouse IgG (Jackson ImmunoResearch Laboratories, West Grove, PA); and Alexa-labeled goat anti-rabbit, anti-mouse, or anti-rat IgG (Invitrogen, Carlsbad, CA). All other chemical reagents were purchased from Sigma-Aldrich and Wako Pure Chemicals (Kyoto, Japan), unless otherwise stated.

Complementary DNAs (cDNAs)

cDNA encoding mouse Git1 was amplified by polymerase chain reaction (PCR) from mouse brain first-strand cDNA. Other cDNAs were provided by the following researchers: human EphA2 was from N. Mochizuki (National Cardiovascular Center, Osaka, Japan), mouse E-cadherin was from M. Takeichi (RIKEN CDB, Kobe, Japan); Venus was from A. Miyawaki (RIKEN BSI, Wako, Japan); mouse Arf1 and Arf6 were from K. Nakayama (Kyoto University), and mouse Nck1 was from T. Shishido (NAIST, Nara, Japan). pcDNA3 FLAG N dest, pcDNA3 HA N dest., and pEBG dest vectors were generated using the Gateway vector conversion kit (Invitrogen). EphA2, Git1, and Nck1 cDNAs were inserted into the pENTR/D topo vector and transferred into their destination vectors by using LR clonaseII (Invitrogen). pBabe puro Arf6-HA, Arf6T27N-HA, Arf6Q67L-HA, and Arf1Q71L-HA were generated by cloning HindIII-XbaI fragments from pcDNA3 Arf6-HA, Arf6T27N-HA, Arf6Q67L-HA, and Arf1Q71L-HA into the SnaBI site of the pBabe puro vector after filling of the ends. pVenus N1 E-cadherin was described previously (Bauer *et al.*, 2008).

Transfections

cDNA transfections were performed using Lipofectamine 2000 (Invitrogen) according to the manufacturer's instructions.

To establish cells stably expressing specific cDNAs, transfection-positive cells were selected by culturing in the presence of the appropriate drugs (4 μg/ml puromycin for the pBabe puro vector or 1 mg/ml G418 for the pcDNA3 and pVenus N1 vectors). Cells were then cloned by limited dilution, and the results were confirmed by at least two independent cell clones for each plasmid.

Small Interfering RNAs

MDCK cells were transfected with oligonucleotide duplexes by using a reverse transfection method, according to the manufacturer's instructions (Invitrogen). Briefly, cells were trypsinized, washed, and suspended in DMEM with 10% fetal calf serum. Then, they were plated onto a plastic dish in the presence of 10 nM oligonucleotide duplexes and Lipofectamine 2000 in Opti-MEM (Invitrogen), Finally, they were incubated for 48 h before being subjected to analysis. Nucleotide sequences used were as follows: for *Git1*, sense 5′-GAGGUGGAUAGAAGAGAAAAU-3′; and for *Nck1*, sense 5′-UCCUGGUGGCGAGUUCGAA-3′. An siRNA duplex with an irrelevant sequence (5′-GCGCGCUUUGUAGGAUUCG-3′) was purchased from Dharmacon RNA Technologies (Lafayette, CO).

For the rescue experiment of the Git1 siRNA treatment, mouse Git1 cDNA, tagged with FLAG, in which the siRNA target sequence was mutated into 5′-GAAGTGGATCGGCGGGAGAAC-3′ was used.

Calcium Switch

Calcium switch was performed according to the method described previously (Zantek *et al.*, 1999). Briefly, 8 mM EGTA was added to MDCK cells cultured at the dense density, and then cells were incubated for a further 30 min at 37°C. The medium was then exchanged with DMEM supplemented with 10% fetal calf serum and 4 mM $CaCl_2$, and cells were further incubated for the times indicated.

GST-Golgi-localizing, Gamma-Adaptin Ear Domain Homology, ARF-binding Protein (GGA) Pulldown, Immunoprecipitation, and Immunoblotting

Arf6 activities were measured using GST-GGA (Santy and Casanova, 2001). Cells were lysed in a lysis buffer (1% Triton X-100, 0.05% sodium cholate, 0.005% SDS, 50 mM Tris-HCl, pH 8.0, 100 mM NaCl, 10 mM $MgCl_2$, 10% glycerol, 2 mM dithiothreitol, 1 mM phenylmethylsulfonyl fluoride, 5 μg/ml aprotinin, 2 μg/ml leupeptin, and 3 μg/ml pepstatin A). After clarifying by centrifugation at 1500 × *g* for 5 min, supernatants were incubated with GST-GGA3 conjugated to glutathione-Sepharose for 40 min at 4°C.

Immunoprecipitation assays were performed using antibodies coupled with protein G-Sepharose, as described previously (Morishige *et al.*, 2008), in which cells were lysed in NP-40 buffer (1% Nonidet P-40, 20 mM Tris-HCl, pH 7.4, 150 mM NaCl, 5 mM EDTA, 1 mM Na_3VO_4, 1 mM phenylmethylsulfonyl fluoride, 5 μg/ml aprotinin, 2 μg/ml leupeptin, and 3 μg/ml pepstatin A). When cells were pretreated with ephrinA1-Fc or control Fc, biotin-conjugated $F(ab')_2$ fragments of goat anti-rabbit or anti-mouse IgG, coupled to streptavidin-Sepharose beads, were used. Three hundred micrograms of cell lysates was used for each GGA pulldown and immunoprecipitation.

Immunoblotting was performed as described previously (Morishige *et al.*, 2008). To enhance the signal from the endogenous Arf6 protein, Can Get Signal (Toyobo Engineering, Osaka, Japan) was used to dilute the anti-Arf6 antibody.

Immunofluorescence Microscopy

Acquisition of confocal images of cells was performed using confocal laser scanning microscopes (LSM510, Carl Zeiss, Jean, Germany and FV1000, Olympus, Tokyo, Japan), as described previously (Mazaki *et al.*, 2001). Z-sections were obtained at 0.5-μm step size. Focuses adjusted across the center of the majority of cell bodies were used to show the localization of E-cadherin, EphA2, Git1-FLAG, Arf-HA, and F-actin. To show the localization of ZO-1, projection images made by summing up all confocal sections into one image were used. Each figure of microscopic analysis shows representative results observed in at least three independent experiments.

RESULTS

Cell Density- and Calcium-dependent Suppression of Arf6 Activity

We first found that the cellular activities of Arf6, measured by the GST-GGA pulldown method (Santy and Casanova,

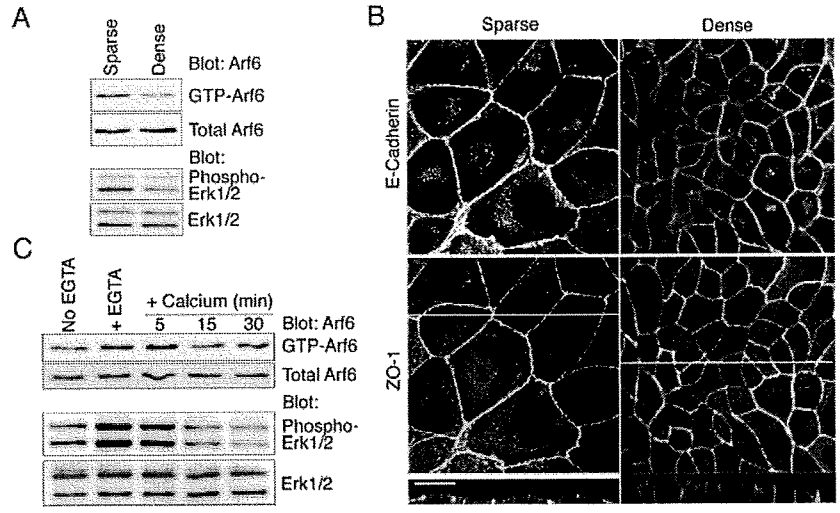

Figure 1. Cell density- and calcium-dependent suppression of Arf6 and Erk1/2 activities in MDCK cells. (A) Arf6 and Erk1/2 activities in cells cultured under dense and sparse densities. Arf6 activities were measured by the GST-GGA pulldown method. Amounts of Arf6 protein in total cell lysates (10 μg) are shown below by immunoblotting. Erk1/2 activities in total cell lysates (10 μg) were assessed by anti-phospho Erk1/2 and anti-Erk1/2 immunoblots, as indicated. (B) Distribution of E-cadherin and ZO-1 in cells cultured under dense and sparse densities. E-cadherin was labeled using the ECCD-2 antibody coupled with an Alexa 488-labeled anti-rat IgG antibody. ZO-1 was labeled using an anti-ZO-1 antibody coupled with an Alexa 555-labeled anti-rabbit IgG antibody. Focuses were adjusted across the center of the majority of cell bodies, for the observation of E-cadherin. Projection images were used for ZO-1. Confocal images of the z-axis (indicated by yellow lines) are also shown at the bottom. Green, E-cadherin; magenta, ZO-1. Bar, 20 μm. (C) Arf6 and Erk1/2 activities during depletion and readdition of calcium ions. Activities of Arf6 and Erk1/2 were assessed as described in A. In A–C, these assays were performed at least three times, and representative figures are shown.

2001), are suppressed in MDCK cells cultured under a dense density as compared with a sparse density, whereas Arf6 protein levels do not notably differ between these two cell densities (Figure 1A). Suppression of Arf6 activity has been implicated in inhibition of the internalization of E-cadherin from cell–cell contact areas, as well as stabilization of the cell–cell contacts (Palacios *et al.*, 2001, 2002). Consistently, E-cadherin seemed to be more densely accumulated at cell–cell contact areas in cells cultured under the dense density than cultured under the sparse density, and this accumulation was accompanied by substantial reduction of the amount of E-cadherin molecules in the cytoplasm and in the apical areas of the cell surface (Figure 1B). Moreover, observation from the z-axis revealed that E-cadherin is more clearly segregated from a tight junction protein, ZO-1, as well as from an apical marker protein, Ezrin, in the dense cells than in the sparse cells (Figure 1B and Supplemental Figure S1), indicating enhanced apical-to-basal polarization of the dense cells compared with the sparse cells.

To obtain clues as to how E-cadherin–based cell–cell adhesions are involved in the suppression of Arf6 activity, we used the calcium switch assay (Zantek *et al.*, 1999), in which calcium ions are first deprived from the culture medium by the addition of EGTA and then added again. We found that Arf6 is swiftly activated upon EGTA treatment and then gradually down-regulated after readdition of calcium (Figure 1C). Activities of Erk1/2 have been shown to be increased by perturbation of E-cadherin–mediated cell–cell contacts in intestinal epithelial cells (Laprise *et al.*, 2004). We confirmed that activities of Erk1/2, as assessed by their phosphorylation, are also increased upon EGTA treatment and then gradually decreased after readdition of calcium in these MDCK cells (Figure 1C; also see below). Likewise, activities of Erk1/2 were suppressed in MDCK cells cultured under a dense density compared with a sparse density (Figure 1A).

Ligand Activation of EphA2 Suppresses Arf6 Activity and Induces Cell Compaction and Polarization

Among the EphA receptors, MDCK cells were found to predominantly express EphA2 (Supplemental Figure S2). We found that tyrosine phosphorylation of EphA2 is dramatically increased in MDCK cells cultured under the dense density compared with the sparse density (Figure 2A). In human mammary epithelial MCF-10A cells, tyrosine phosphorylation of EphA2 has been shown to be dependent on calcium ions in the culture medium (Zantek *et al.*, 1999). Consistently, tyrosine phosphorylation of EphA2 in MDCK cells, which was induced by culturing cells under the dense density, was substantially diminished upon EGTA treatment and was gradually recovered after readdition of calcium (Figure 2B). MDCK cells also express ephrinA1, and, to a lesser extent, ephrinA4 (Supplemental Figure S2), and the above-described enhanced activation of EphA2 under the dense cell density is likely to be due to paracrine stimulation of EphA2 by its ligands upon cell–cell contacting, which might occur more efficiently at the dense cell density than at the sparse cell density. In contrast, ephrins themselves are also known to transduce intracellular signals, upon binding to Eph receptors (Pasquale, 2005). We found that stimulation of MDCK cells, cultured under the sparse density, with ephrinA1 fused to the Fc portion of human immunoglobulin G (ephrinA1-Fc) down-regulates Arf6 activity, whereas a control Fc fragment or EphA2-Fc did not (Figure 2C). Dense tyrosine phosphorylation of EphA2 upon ephrinA1-Fc stimulation was confirmed under the same condition (data not shown). This ephrinA1-Fc stimulation of MDCK cells also induced cell compaction, which was accompanied by the enhanced accumulation of E-cadherin to cell–cell contact areas (Figure 2, D and E, Supplemental Figure S3 and Supplemental Video S1). Observation from the z-axis revealed that E-cadherin is more clearly segregated from ZO-1 and Ezrin in ephrinA1-Fc–treated cells than in control Fc-treated cells, indicating that these ephrinA1–Fc-treated cells were more polarized in the apical-to-basal direction, as seen with cells cultured under the dense density (Figure 2D and Supplemental Figure S1). Therefore, ephrinA1-stimulated MDCK cells resemble those cells cultured under the dense density, in their EphA2 phosphorylation, Arf6 activities, morphology and apical-to-basal polarization. We also found that treatment of MDCK cells with an anti-E-cadherin antibody, DECMA-1, which blocks E-cadherin function (Vestweber and Kemler, 1985), inhibits ephrinA1–Fc-mediated cell compaction (Figure 2F), suggesting the involvement of homophilic E-cadherin adhesion in this event.

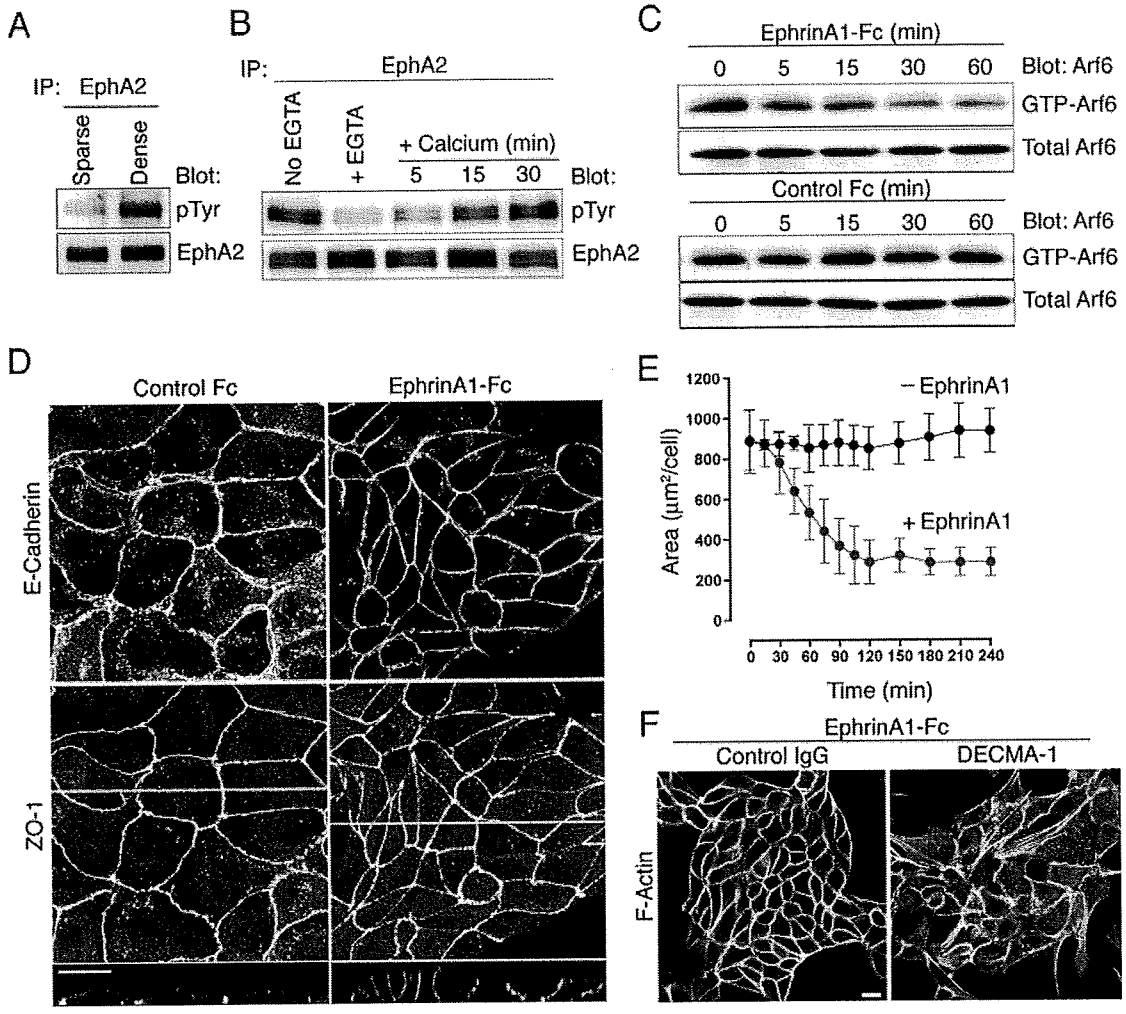

Figure 2. EphrinA1 stimulation causes Arf6 suppression, cell compaction, and apical-basal polarization in MDCK cells. (A and B) Tyrosine phosphorylation of EphA2 in cells cultured under dense and sparse densities (A) or during depletion and readdition of calcium ions (B) was assessed by immunoblotting as indicated. (C) Arf6 activities in cells cultured under the sparse density and treated with ephrinA1-Fc or control Fc for the indicated times. (D) E-Cadherin and ZO-1 distribution, as well as cell morphology, in cells treated with ephrinA1-Fc or control Fc for 3 h. Confocal images of the z-axis, indicated by yellow lines, are shown at the bottom. E-Cadherin and ZO-1 were visualized as shown in Figure 1B. (E) Time course of cell compaction upon ephrinA1 treatment. Cells expressing E-cadherin-Venus and cultured under the sparse density were subjected to time-lapse imaging in the presence or absence of ephrinA1-Fc, and their surface areas, as determined by E-cadherin-Venus–positive cell–cell junctions, were calculated. Error bars represent ± SEM from three independent experiments (n = 5 in each experiment). (F) Inhibition of ephrinA1-induced cell compaction by the DECMA-1 antibody. Cells cultured under the sparse density were pretreated with DECMA-1 (25 μg/ml) or control IgG for 30 min and then stimulated with ephrinA1-Fc for 3 h in the presence of DECMA-1 or IgG. Rhodamine-phalloidin staining of cells are shown. In A, B, and C, each assay was performed three times, and representative figures are shown. Total, 10 μg of total cell lysates. Bars 20 μm (D and F).

Dominant-Active Form of Arf6 Blocks EphrinA1-induced Cell Compaction

To assess whether ephrinA1–Fc-induced cell compaction is related to Arf6 activities, we next established MDCK cell lines stably expressing HA-tagged Arf6 and its mutants (Figure 3A). Expression of a guanosine triphosphate (GTP) hydrolysis-defective form of Arf6-HA, Arf6Q67L-HA, but not wild-type Arf6-HA, caused a spread out cell morphology, which was resistant to ephrinA1–Fc-mediated cell compaction (Figure 3, B and C). Such resistance to ephrinA1-Fc was not observed with a similar type of Arf1 mutant, Arf1Q71L-HA (Figure 3, B and C). In contrast, expression of a GTP binding-defective form of Arf6-HA, Arf6T27N-HA, induced cell compaction (Figure 3, A–C). However, expression of Arf6T27N-HA was very low compared with wild-type Arf6-HA and Arf6Q67L-HA (Figure 3A), and these cells expressing Arf6T27N-HA could respond to ephrinA1-Fc to become more compacted (Figure 3, B and C). These results are consistent with the notion that down-regulation of Arf6 activity plays an integral role in the pathway by which ligand-activated EphA2 induces cell compaction.

EphA2 Uses Git1 to Suppress Arf6 Activity

We then sought to clarify the mechanism by which ligand-activated EphA2 down-regulates Arf6 activity. EphA2 signaling pathways have already been extensively characterized (Pasquale, 2005). However, none of the known signaling pathways can adequately explain the suppression

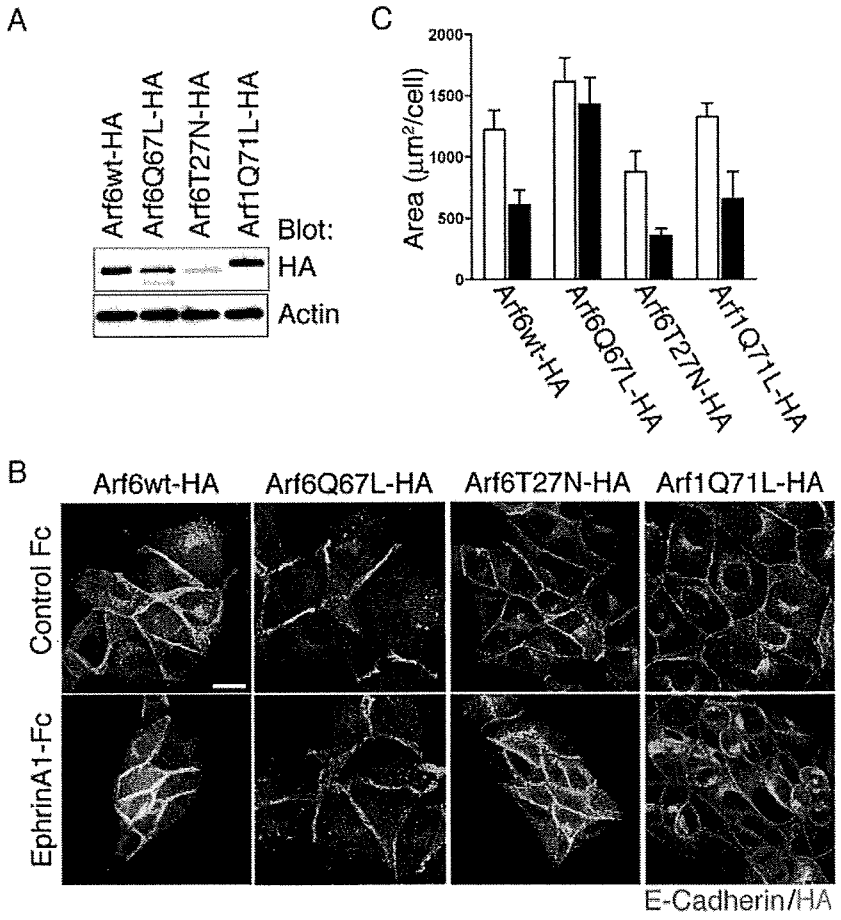

Figure 3. Arf6Q67L blocks ephrinA1-induced cell compaction in MDCK cells. (A) Expression of Arf6-HA, its mutants or Arf1Q71L-HA, as detected by anti-HA immunoblots. Anti-actin immunoblots are included as a control. (B and C) Morphology and E-cadherin distribution (B) and surface areas (C) of cells expressing HA-tagged Arf proteins and treated with ephrinA1-Fc or control Fc for 3 h. In B, E-cadherin was labeled by the ECCD-2 antibody coupled with an Alexa 555-labeled anti-rat IgG antibody (magenta) and HA-Arfs by an anti-HA antibody coupled with an Alexa 488-labeled anti-mouse IgG antibody (green). Bar, 20 μm. In C, open bars, control Fc; closed bars, ephrinA1-Fc. Error bars represent ± SEM from three independent experiments (n = 30 in each experiment).

of Arf6 by EphA2. We examined whether some GTPase activation proteins (GAPs) for Arf GTPases are linked to EphA2. Git1 exhibits efficient GAP activity against different Arf isoforms, including Arf6 (Premont *et al.*, 1998; Meyer *et al.*, 2006). We found that a significant amount of Git1 is coimmunoprecipitated with EphA2, when MDCK cells are stimulated by ephrinA1-Fc (Figure 4A). Conversely, an anti-Git1 antibody also coimmunoprecipitated significant amounts of EphA2, which was dependent on ephrinA1-Fc stimulation (Figure 4B). Git1 has a structurally conserved isoform, namely, Git2 (Hoefen and Berk, 2006). Git2 did not coprecipitate with EphA2 (Figure 4A). Consistent with these results, siRNA-mediated knockdown of Git1 substantially abolished ephrinA1–Fc-mediated suppression of Arf6 activity, as well as ephrinA1–Fc-mediated cell compaction and apical-to-basal polarization (Figure 4, C–F and Supplemental Figure S4). To confirm the specificity of the Git1 siRNA, we then established MDCK cells expressing a rescue construct of Git1-FLAG, in which the Git1 siRNA-target nucleotides were mutated (Figure 4C), and we confirmed that ephrinA1–Fc-mediated suppression of Arf6 activity, as well as ephrinA1–Fc-mediated cell compaction were still observed in these "rescued" cells, even when the cells were treated with the Git1 siRNA (Figure 4, D–F). These results suggest that EphA2, when ligand activated, uses Git1 to suppress Arf6 activity and that this engagement of Git1 is important for the EphA2-mediated modulation of cell–cell contacts.

Ligand-activated EphA2 is known to attenuate the activities of mitogen-activated protein kinases (Miao *et al.*, 2001). Moreover, the Arf6 GTPase cycle has been implicated in the activation of Erk kinases (Tague *et al.*, 2004). We however found that knockdown of Git1 does not affect ephrinA1–Fc-induced suppression of Erk1/2 activities (Figure 4D). Therefore, the EphA2–Git1 pathway down-regulating Arf6 activity is substantially independent of the EphA2 pathway down-regulating Erk1/2 activity in MDCK cells.

EphA2 Requires Nck1 to Associate with Git1

Git1 does not seem to have protein interaction modules that can directly bind to ligand activated EphA2. In contrast, Git1 has been shown to bind to several adaptor proteins, such as Nck (Frese *et al.*, 2006). Among the Nck isoforms, MDCK cells predominantly express Nck1 (Supplemental Figure S1). We found that Nck1 is readily coprecipitated with Git1 in MDCK cells even without ephrinA1-Fc stimulation (Figure 5A). In contrast, Nck1 coprecipitated with EphA2 only after ephrinA1-Fc stimulation of these cells (Figure 5A). Coprecipitation of Git1 with EphA2 was abolished upon siRNA-mediated knockdown of Nck1 (Figure 5, B and C). Similar to the Git1 knockdown, knockdown of Nck1 also abolished ephrinA1-Fc-mediated suppression of Arf6 activity (Figure 5D), as well as ephrinA1–Fc-mediated cell compaction and apical-to-basal polarization (Figure 5, E and F, and Supplemental Figure S4). Therefore, Nck1 seems to link Git1 with ligand-activated EphA2.

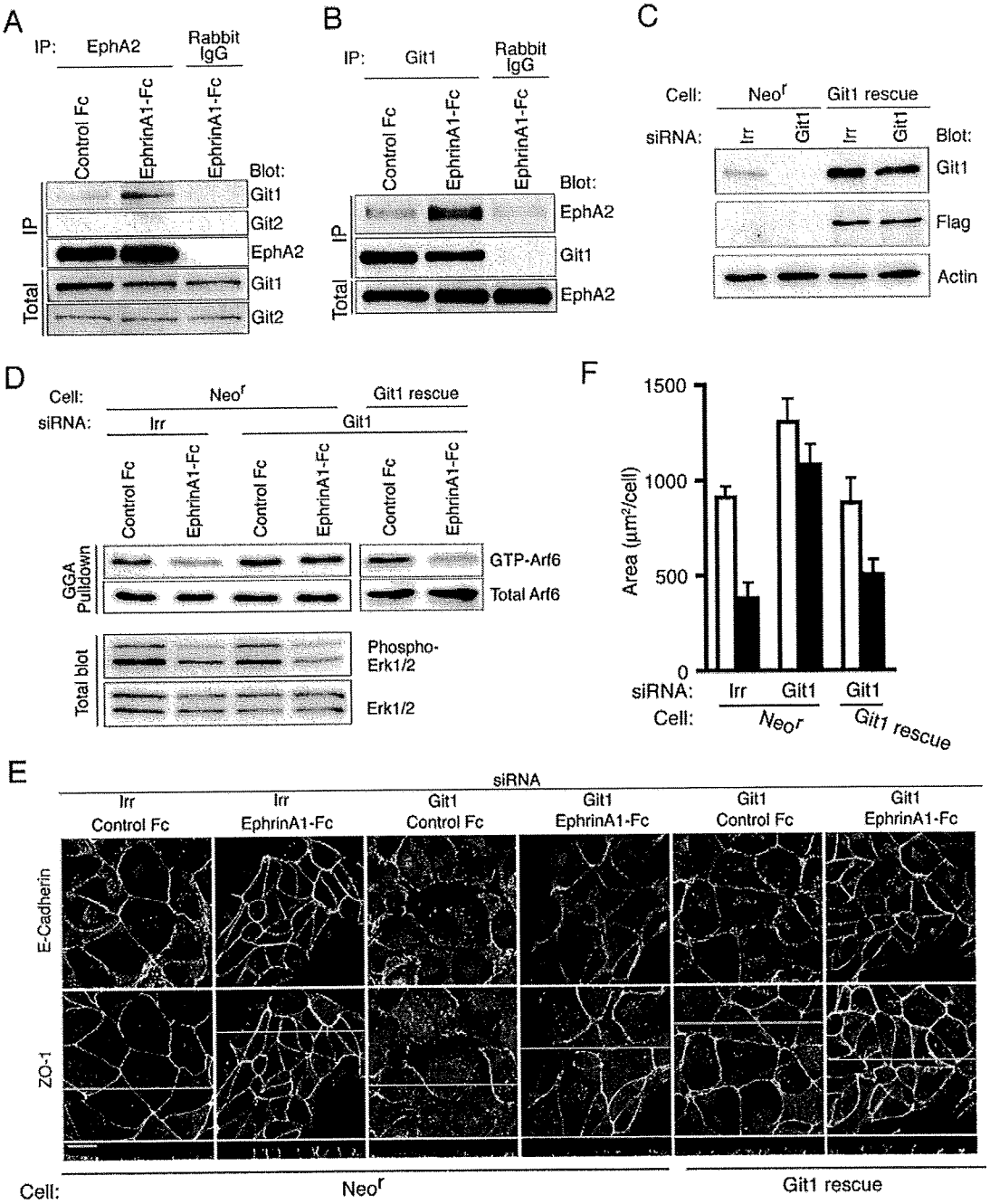

Figure 4. EphA2 requires Git1 for Arf6 suppression and cell compaction in MDCK cells. (A and B) Coprecipitation of Git1 with EphA2 upon ephrinA1-Fc stimulation. Cells cultured under the sparse density were stimulated with ephrinA1-Fc or control Fc for 30 min, and their EphA2 (A) or Git1 (B) was immunoprecipitated and analyzed for the coprecipitation of Git1 (A) and EphA2 (B) by immunoblotting, as indicated. Controls include nonspecific IgGs (rabbit IgG) and an anti-Git2 antibody, as indicated. (C–F) Requirement of Git1 for Arf6 suppression (D), and cell compaction (E and F), induced by ephrinA1-Fc. Cells stably transfected with pcDNA3 (Neo^r) or the FLAG-tagged Git1 rescue plasmid (Git1 rescue) were treated with Git1 siRNA or an irrelevant siRNA (Irr) and cultured under the sparse density. In D, cells were treated with ephrinA1-Fc or control Fc for 30 min. In E and F, cells were treated with ephrinA1-Fc or control Fc for 3 h. Endogenous Git1 and rescue Git1 expression (C) and cell surface areas (F) are also shown. In D, Erk1/2 activities in total cell lysates (10 μg) were assessed by anti-phospho-Erk1/2 and anti-Erk1/2 immunoblots, as indicated. In E, E-cadherin and ZO-1were labeled as described in Figure 1. Confocal images of the z-axis, indicated by yellow lines, are shown at the bottom. Bar, 20 μm. In F, open bars, control Fc; closed bars, ephrinA1-Fc. Other labels are the same as in Figures 1 and 2.

Precise Mechanisms of Formation of the EphA2–Nck1–Git1 Complex

The above-mentioned results indicate that the association of Nck1 and EphA2 occurs only after ephrinA1 stimulation, whereas that of Nck1 and Git1 occurs constitutively. We then investigated the precise mechanisms involved in the protein interactions of this EphA2–Nck1–Git1 complex. Because EphA2 makes a complex with Git1 upon ephrinA1-Fc

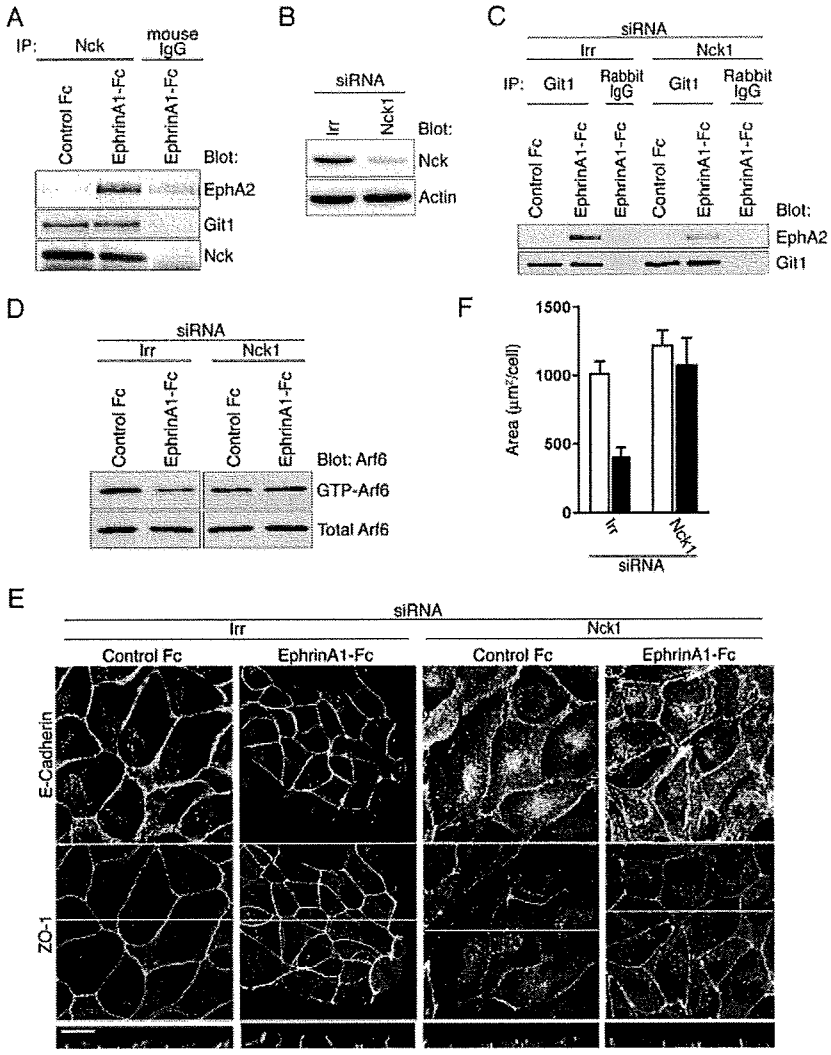

Figure 5. Nck links EphA2 with Git1 in MDCK cells. (A) Complex formation of Nck with EphA2 and Git1. Cells cultured under the sparse density were stimulated with EphrinA1-Fc or control Fc for 30 min, immunoprecipitated with an anti-Nck antibody and analyzed for coprecipitation of EphA2 and Git1 by immunoblotting, as indicated. Nonspecific IgGs (mouse IgG) were included as a control. (B–F) Cells were treated with an Nck1 siRNA or an irrelevant siRNA (Irr) and cultured under the sparse density. Requirement for Nck1 in EphA2-Git1 association (C), Arf6 suppression (D), E-cadherin and ZO-1 localization (E), and cell compaction (F), induced by ephrinA1-Fc, are shown. In C and D, cells were treated with ephrinA1-Fc or control Fc for 30 min. In E and F, cells were treated with ephrinA1-Fc or control Fc for 3 h. Nck1 expression in total cell lysates (10 μg) is also shown (B). In C, nonspecific IgGs (Rabbit IgG) are included as a control. In E, confocal images of the z-axis, indicated by yellow lines, are shown at the bottom. Bar, 20 μm. In F, open bars, control Fc; closed bars, ephrinA1-Fc. Other labels are the same as in Figures 1 and 2.

stimulation, we first examined the possible involvement of ligand-induced tyrosine phosphorylation of EphA2 in this complex formation. Phosphorylation of highly conserved tyrosine residues on the juxtamembrane region of Eph receptors, which correspond to Tyr588 and Tyr594 of EphA2, has been shown to be the major Nck binding sites (Kullander and Klein, 2002). We expressed Git1-FLAG in HEK293T cells together with HA-tagged EphA2 (EphA2-HA) or its tyrosine nonphosphorylation mutants Y588F and Y594F, in which Tyr588 and Tyr594 are mutated into phenylalanine, respectively (Figure 6A). HEK293T cells express Nck endogenously (Figure 6B). Moreover, EphA2 overexpressed in HEK293T cells was notably tyrosine-phosphorylated even without exogenous stimulation by ephrinA1-Fc (data not shown), similar to those observed with other Eph receptors overexpressed in HEK293 cells (Becker *et al.*, 2000). We found that mutation of Tyr594, but not Tyr588, substantially abolishes coprecipitation of EphA2-HA with Git1-FLAG (Figure 6B). We then examined whether phosphorylation of Tyr594 is necessary for the association of EphA2 with Nck1. Nck1 has one Src homology 2 (SH2) domain, a domain known to bind to phosphotyrosines. We found that a GST fusion form of the SH2 domain of Nck1 (GST-Nck1 SH2) binds to wild-type EphA2-HA and its Y588F mutant (EphA2 Y588F-HA) but not the Y594F mutant (EphA2 Y594F-HA) (Figure 6C).

We next investigated which portion(s) of Git1 is necessary for its complex formation with EphA2. It has been reported that Tyr392 of Git1 can be phosphorylated and that this phosphorylation enables its binding to the SH2 domain of Nck (Frese *et al.*, 2006). We however found that mutation of Tyr392 into phenylalanine (Git1Y392F-FLAG) does not affect its complex formation with EphA2-HA (Figure 6D). In contrast, we showed above that EphA2 does not associate with Git2 (Figure 6D). The synaptic localizing domain, present in Git1, is not well conserved in Git2 (Supplemental Figure S5). We found that the synaptic localizing domain-deletion mutant of Git1 (Git1ΔSLD-FLAG) no longer associates with EphA2-HA (Figure 6D). Consistently, the synaptic localizing domain of Git1 alone (Git1 SLD-FLAG) was able to associate with EphA2-HA (Figure 6D). The synaptic localizing domain of Git1 contains several repeats of proline-rich sequences at its C terminus, which apparently conform to Src homology 3 (SH3) binding motifs. Nck1 contains three tandem repeats of SH3 domains. Deletion of these proline-rich regions from the synaptic localizing domain of Git1 (Git1 SLDΔC-FLAG) abolished its complex formation with

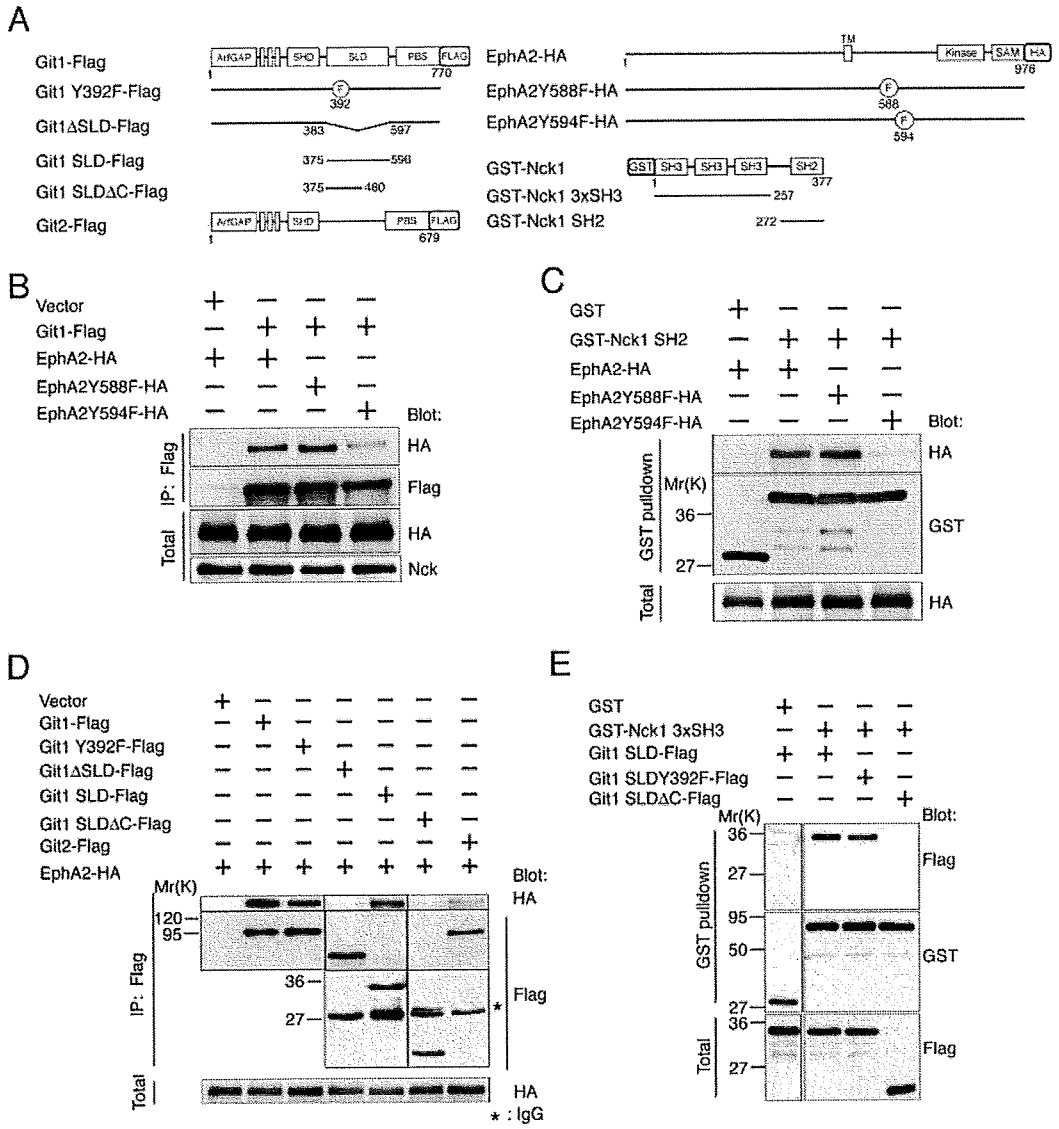

Figure 6. Mechanism of EphA2–Nck1–Git1 complex formation. (A) Schematic representations of EphA2, Nck1, Git1, and their mutants. (B) Requirement for Tyr594 of EphA2 in EphA2-Git1 complex formation. Git1-FLAG was coexpressed with EphA2-HA or its YF mutants in HEK293T cells, as indicated, and immunoprecipitated with an anti-FLAG antibody to analyze its association with EphA2 mutants. (C) Binding of EphA2 to the Nck1 SH2 domain. GST-Nck1 SH2 was coexpressed with EphA2-HA or its YF mutants in HEK293T cells, as indicated, and subjected to GST pulldown to analyze its association with EphA2 mutants. (D) Requirement of the synaptic localizing domain of Git1 in EphA2-Git1 complex formation. Git1-FLAG or its mutants were coexpressed with EphA2-HA in HEK293T cells, as indicated, and immunoprecipitated with an anti-FLAG antibody to analyze their association with EphA2. Git2-FLAG is also included as a control. (E) Binding of the Git1 synaptic localizing domain to the Nck1 SH3 domains. GST-Nck1 3xSH3 (three tandem SH3 domains of Nck1) was coexpressed with Git1 SLD-FLAG or its mutants in HEK293T cells, as indicated, and subjected to GST pulldown to analyze its association with the Git1 synaptic localizing domain and its mutants. In B–E, total, 10 μg of total cell lysates. GST or empty vector are also included as controls.

EphA2-HA (Figure 6D). We also confirmed that the SH3 domains of Nck1, fused to GST (GST-Nck1 3xSH3), bind to Git1 SLD-FLAG but not Git1 SLDΔC-FLAG (Figure 6E). Together, it is most likely that in the EphA2–Nck1–Git1 complex, the phosphorylated Tyr594 of EphA2 binds to the SH2 domain of Nck1, and the SH3 domains of Nck1 bind to the synaptic localizing domain of Git1. Our results also indicate that Tyr392 of Git1 is dispensable for its association with EphA2. Tyr392 is conserved in Git2, whereas the synaptic localizing domain is not. Lack of the synaptic localizing domain in Git2 may explain why Git2 is not directly engaged by EphA2.

Subcellular Distribution of Git1 and EphA2 in MDCK Cells

We finally examined the possible colocalization of Git1, and also its mutants, with EphA2. Because immunostaining of endogenous Git1 in MDCK cells was very weak, we stably expressed Git1-FLAG and its mutants in MDCK cells and visualized them by use of an anti-FLAG antibody (Figure 7A). EphA2 is known to localize to cell–cell contact areas (Zantek *et al.*, 1999). We found that although only a small amount of Git1-FLAG is localized to cell–cell contact areas when cells are cultured under the sparse density, a significant fraction is swiftly recruited to cell–cell contact areas

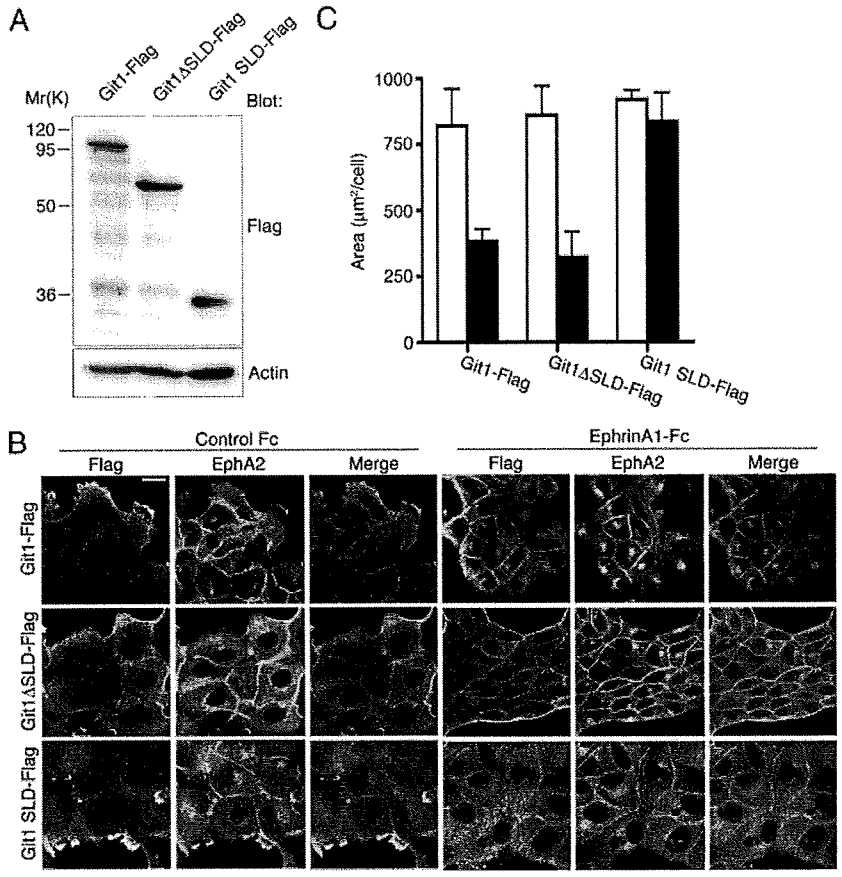

Figure 7. Subcellular localization of EphA2 and Git1 in MDCK cells. (A) Expression of Git1-FLAG or its mutants, as detected by anti-FLAG immunoblots of total cell lysates (10 μg). Anti-actin immunoblots are shown as a control. (B and C) Colocalization of Git1, and its mutants, with EphA2 in ephrinA1-Fc-treated MDCK cells (B), and their effects on cell compaction (C). Cells stably expressing Git1-FLAG or its mutants were cultured under the sparse density and treated with ephrinA1-Fc or control Fc for 1 h, before being labeled with an anti-FLAG antibody coupled with an Alexa 488-labeled anti-mouse IgG antibody (green) and an anti-EphA2 antibody coupled with an Alexa 555-labeled anti-rabbit IgG antibody (magenta). Bar, 20 μm (B). In C, open bars, control Fc; closed bars, ephrinA1-Fc.

upon ephrinA1-Fc stimulation and colocalizes well with EphA2 (Figure 7B). The synaptic localizing domain of Git1 was previously identified as being responsible for its localization to neuronal synapses (Zhang *et al.*, 2003). In MDCK cells, however, we found that Git1ΔSLD-FLAG, which lacks the synaptic localizing domain, is still able to localize to cell–cell contacts, although with a lower efficiency than that of intact Git1-FLAG (Figure 7, B and C). In contrast, expression of the synaptic localizing domain alone (Git1 SLD-FLAG) blocked ephrinA1–Fc-mediated cell compaction, whereas this domain alone seemed to be very inefficient in localizing to the cell–cell contacts (Figure 7, B and C). These results again suggest the importance of the synaptic localizing domain of Git1 in Eph signaling, although this domain per se is not essential for its localization to cell–cell contacts.

DISCUSSION

EphA receptors have been implicated in the inhibition of cell migration and growth. To accomplish such roles, several EphA receptors have been shown to employ signaling molecules that down-regulate the activities of Ras and Rac small GTPases, such as p120RasGAP and α-chimaerin (Pasquale, 2005, 2008). In this paper, we show that EphA2 has a novel signaling pathway that downregulates the activity of another small GTPase, Arf6, by recruiting Git1. Through this pathway, we show that the ligand-activation of EphA2, which may occur during cell-cell contacting of epithelial cells, contributes to the cell compaction as well as the maturation of E-cadherin-based cell-cell adhesion and apical-basal polarization. Our results also show that E-cadherin function is necessary for the EphA2-mediated down-regulation of the Arf6 activity during cell-cell contacting. Therefore, it is plausible to assume that a positive feedback loop exists between EphA2 and E-cadherin in some normal epithelial cells, in which E-cadherin-based cell-cell contacts enhance binding of EphA2 receptors with their ligands, which in turn activates the signaling pathway at the cell-cell contacting areas to down-regulate Arf6 activity, and this down-regulation then acts to enhance E-cadherin-based cell-cell adhesions as well as maturation of apical-basal polarization.

Git1 has been shown to localize and function at cell–cell junctions formed in neuronal synapses (Zhang *et al.*, 2003) and immune synapses (Phee *et al.*, 2005). However, these studies have mostly dealt with Git1 as a scaffold protein, which links cell surface receptors to the Pix–Pak pathway to remodel actin cytoskeletal architecture and stabilize these cell–cell junctions. In contrast, our present study clarifies the role of Git1 as a GTPase-activating protein for Arf6 in the stabilization of cell–cell junctions.

We show that EphA2 signaling causes enhanced polarization in the apical-to-basal direction, which is accompanied by clear segregation of ZO-1 and Ezrin from E-cadherin. Interestingly, suppression of Git1 and Nck1 expression also affects the subcellular localization of ZO-1. Therefore, activation of the EphA2–Nck1–Git1 signaling pathway seems to lead to maturation of tight junction structures, together with the maturation of adherens junctions. In contrast, it has been shown that an active form of the Arf6 mutant does not

perturb localization of ZO-1 at cell–cell contacts in MDCK cells under a condition in which this mutant disrupts E-cadherin–based adherens junctions (Palacios *et al.*, 2001). It will be interesting to investigate whether the EphA2–Nck1–Git1 pathway, as well as the GAP activity of Git1, is directly involved also in the maturation of tight junctions. Moreover, Eph receptor signaling also regulates activities of other small GTPases, including Rac1, RhoA, and Rap1 (Pasquale, 2005), which may also be involved in modulating the architecture of cell–cell adhesions. In particular, it has been shown that Rac1 activities can be tightly coupled with activities of Arf6 (Radhakrishna *et al.*, 1999). It will be interesting to examine whether EphA2 signaling, as well as cell densities affect activities of other small GTPases.

Penela *et al.* (2008) have reported that Git1 plays a role in enhancing cell migration and proliferation of HeLa cells and COS7 cells, by interacting with G protein-coupled receptor kinase 2. These cells are completely transformed; moreover, HeLa cells have lost the expression of E-cadherin. Their report, together with our results suggest that Git1 may be pleiotropic, having different roles in different signaling pathways or cellular contexts. It will be interesting to examine whether Git1 also acts as a GAP for Arf6 in G protein-coupled receptor signaling or just acts as a scaffold protein in this signaling pathway.

The synaptic localizing domain of Git1 contains both typical and atypical PXXP motifs at its C terminus and has been predicted to bind to some yet unidentified SH3 domains (Bagrodia *et al.*, 1999). We show that the Nck1 SH3 domain binds to this synaptic localizing domain, an interaction which requires the C-terminal proline-rich region of this synaptic localizing domain. Recently, it was reported that Git1 forms a closed conformation by intramolecular interaction between its N- and C-terminal regions. When the synaptic localizing domain or the Ankyrin repeat is deleted, Git1 seems to change to an open conformation and shows increased affinities to paxillin and liprin α (Totaro *et al.*, 2007). We observed that the synaptic localizing domain of Git1 alone shows higher affinity to the Nck SH3 domain than full-length Git1 (data not shown). Therefore, it will be interesting to examine whether Eph signals have a role in changing Git1 to an open conformation and hence up-regulating its binding to other proteins. It will also be interesting to examine whether Eph signals up-regulate the GAP activity of Git1.

Disruption of E-cadherin–mediated cell–cell adhesions is the major cause for the acquisition of invasive and metastatic properties in most types of carcinomas (Takeichi, 1991). The *EphA2* gene has been implicated in tumor suppression, as mentioned. It will thus be interesting to clarify the precise molecular mechanism by which Arf6 activity, which is under the regulation of the EphA2–Nck–Git1 signaling pathway, participates in the processes maintaining E-cadherin–mediated cell–cell adhesions, especially those regulating the cellular dynamics and fates of E-cadherin molecules. Moreover, loss of EphB receptors have also been highly implicated in the tumorigenesis of different types of cancers (Pasquale, 2008), and EphB signaling has also been shown to enhance cell–cell adhesion by recruiting E-cadherin to the plasma membrane (Cortina *et al.*, 2007). Furthermore, EphB receptors possess Nck SH2 binding sites (Kullander and Klein, 2002). It will thus be interesting to examine whether EphB receptors also use a similar pathway involving the suppression of Arf6 activity.

ACKNOWLEDGMENTS

We are grateful to T. Yoneda, Y. Shibata, A. Arakawa, M. Minamimoto, and M. Hiraishi for technical assistance and Y. Okuda for secretarial work. We also thank M. Takeichi, A. Miyawaki, K. Nakayama, and T. Shishido for cDNAs; Sh. Tsukita for cells; Y. Mazaki and A. Suzuki for technical suggestions; and H. A. Popiel for critical reading of the manuscript. This work was supported in part by grants-in-aid from the Ministry of Education, Science, Sports and Culture of Japan and by the Takeda Science Foundation.

REFERENCES

Bagrodia, S., Bailey, D., Lenard, Z., Hart, M., Guan, J. L., Premont, R. T., Taylor, S. J., and Cerione, R. A. (1999). A tyrosine-phosphorylated protein that binds to an important regulatory region on the cool family of p21-activated kinase-binding proteins. J. Biol. Chem. *274*, 22393–22400.

Bauer, T., Motosugi, N., Miura, K., Sabe, H., and Hiiragi, T. (2008). Dynamic rearrangement of surface proteins is essential for cytokinesis. Genesis *46*, 152–162.

Becker, E., Huynh-Do, U., Holland, S., Pawson, T., Daniel, T. O., and Skolnik, E. Y. (2000). Nck-interacting Ste20 kinase couples Eph receptors to c-Jun N-terminal kinase and integrin activation. Mol. Cell. Biol. *20*, 1537–1545.

Cortina, C., *et al.* (2007). EphB-ephrin-B interactions suppress colorectal cancer progression by compartmentalizing tumor cells. Nat. Genet. *39*, 1376–1383.

Donaldson, J. G. (2003). Multiple roles for Arf *6*, sorting, structuring, and signaling at the plasma membrane. J. Biol. Chem. *278*, 41573–41576.

Frese, S., Schubert, W. D., Findeis, A. C., Marquardt, T., Roske, Y. S., Stradal, T. E., and Heinz, D. W. (2006). The phosphotyrosine peptide binding specificity of Nck1 and Nck2 Src homology 2 domains. J. Biol. Chem. *281*, 18236–18245.

Gumbiner, B. M. (2005). Regulation of cadherin-mediated adhesion in morphogenesis. Nat. Rev. Mol. Cell Biol. *6*, 622–634.

Guo, H., Miao, H., Gerber, L., Singh, J., Denning, M. F., Gilliam, A. C., and Wang, B. (2006). Disruption of EphA2 receptor tyrosine kinase leads to increased susceptibility to carcinogenesis in mouse skin. Cancer Res. *66*, 7050–7058.

Hiroi, T., Someya, A., Thompson, W., Moss, J., and Vaughan, M. (2006). GEP100/BRAG 2, activator of ADP-ribosylation factor 6 for regulation of cell adhesion and actin cytoskeleton via E-cadherin and α-catenin. Proc. Natl. Acad. Sci. USA *103*, 10672–10677.

Hoefen, R. J., and Berk, B. C. (2006). The multifunctional GIT family of proteins. J. Cell Sci. *119*, 1469–1475.

Kullander, K., and Klein, R. (2002). Mechanisms and functions of Eph and ephrin signalling. Nat. Rev. Mol. Cell Biol. *3*, 475–486.

Laprise, P., Langlois, M. J., Boucher, M. J., Jobin, C., and Rivard, N. (2004). Down-regulation of MEK/ERK signaling by E-cadherin-dependent PI3K/Akt pathway in differentiating intestinal epithelial cells. J. Cell. Physiol. *199*, 32–39.

Macrae, M., Neve, R. M., Rodriguez-Viciana, P., Haqq, C., Yeh, J., Chen, C., Gray, J. W., and McCormick, F. (2005). A conditional feedback loop regulates Ras activity through EphA2. Cancer Cell *8*, 111–118.

Mazaki, Y., *et al.* (2001). An ADP-ribosylation factor GTPase-activating protein Git2-short/KIAA0148 is involved in subcellular localization of paxillin and actin cytoskeletal organization. Mol. Biol. Cell *12*, 645–662.

Meyer, M. Z., Deliot, N., Chasserot-Golaz, S., Premont, R. T., Bader, M. F., and Vitale, N. (2006). Regulation of neuroendocrine exocytosis by the ARF6 GTPase-activating protein GIT1. J. Biol. Chem. *281*, 7919–7926.

Miao, H., Burnett, E., Kinch, M., Simon, E., and Wang, B. (2000). Activation of EphA2 kinase suppresses integrin function and causes focal-adhesion-kinase dephosphorylation. Nat. Cell Biol. *2*, 62–69.

Miao, H., Nickel, C. H., Cantley, L. G., Bruggeman, L. A., Bennardo, L. N., and Wang, B. (2003). EphA kinase activation regulates HGF-induced epithelial branching morphogenesis. J. Cell Biol. *162*, 1281–1292.

Miao, H., Wei, B. R., Peehl, D. M., Li, Q., Alexandrou, T., Schelling, J. R., Rhim, J. S., Sedor, J. R., Burnett, E., and Wang, B. (2001). Activation of EphA receptor tyrosine kinase inhibits the Ras/MAPK pathway. Nat. Cell Biol. *3*, 527–530.

Morishige, M., *et al.* (2008). GEP100 links epidermal growth factor receptor signalling to Arf6 activation to induce breast cancer invasion. Nat. Cell Biol. *10*, 85–92.

Noblitt, L. W., Bangari, D. S., Shukla, S., Knapp, D. W., Mohammed, S., Kinch, M. S., and Mittal, S. K. (2004). Decreased tumorigenic potential of EphA2-overexpressing breast cancer cells following treatment with adenoviral vectors that express EphrinA1. Cancer Gene Ther. *11*, 757–766.

Noren, N. K., Foos, G., Hauser, C. A., and Pasquale, E. B. (2006). The EphB4 receptor suppresses breast cancer cell tumorigenicity through an Abl-Crk pathway. Nat. Cell Biol. *8*, 815–825.

Palacios, F., Price, L., Schweitzer, J., Collard, J. G., and D'Souza-Schorey, C. (2001). An essential role for ARF6-regulated membrane traffic in adherens junction turnover and epithelial cell migration. EMBO J. *20*, 4973–4986.

Palacios, F., Schweitzer, J. K., Boshans, R. L., and D'Souza-Schorey, C. (2002). ARF6-GTP recruits Nm23–H1 to facilitate dynamin-mediated endocytosis during adherens junctions disassembly. Nat. Cell Biol. *4*, 929–936.

Pasquale, E. B. (2005). Eph receptor signalling casts a wide net on cell behaviour. Nat. Rev. Mol. Cell Biol. *6*, 462–475.

Pasquale, E. B. (2008). Eph-Ephrin bidirectional signaling in physiology and disease. Cell *133*, 38–52.

Penela, P., Ribas, C., Aymerich, I., Eijkelkamp, N., Barreiro, O., Heijnen, C. J., Kavelaars, A., Sanchez-Madrid, F., and Mayor, F., Jr. (2008). G protein-coupled receptor kinase 2 positively regulates epithelial cell migration. EMBO J. *27*, 1206–1218.

Phee, H., Abraham, R. T., and Weiss, A. (2005). Dynamic recruitment of PAK1 to the immunological synapse is mediated by PIX independently of SLP-76 and Vav1. Nat. Immunol. *6*, 608–617.

Premont, R. T., Claing, A., Vitale, N., Freeman, J. L., Pitcher, J. A., Patton, W. A., Moss, J., Vaughan, M., and Lefkowitz, R. J. (1998). β2-Adrenergic receptor regulation by GIT1, a G protein-coupled receptor kinase-associated ADP ribosylation factor GTPase-activating protein. Proc. Natl. Acad. Sci. USA *95*, 14082–14087.

Radhakrishna, H., Al Awar, O., Khachikian, Z., and Donaldson, J. G. (1999). ARF6 requirement for Rac ruffling suggests a role for membrane trafficking in cortical actin rearrangements. J. Cell Sci. *112*, 855–866.

Ruiz, J. C., and Robertson, E. J. (1994). The expression of the receptor-protein tyrosine kinase gene, eck, is highly restricted during early mouse development. Mech. Dev. *46*, 87–100.

Santy, L. C., and Casanova, J. E. (2001). Activation of ARF6 by ARNO stimulates epithelial cell migration through downstream activation of both Rac1 and phospholipase D. J. Cell Biol. *154*, 599–610.

Surawska, H., Ma, P. C., and Salgia, R. (2004). The role of ephrins and Eph receptors in cancer. Cytokine Growth Factor Rev. *15*, 419–433.

Suzuki, T., *et al.* (2006). Crucial role of the small GTPase ARF6 in hepatic cord formation during liver development. Mol. Cell. Biol. *26*, 6149–6156.

Tague, S. E., Muralidharan, V., and D'Souza-Schorey, C. (2004). ADP-ribosylation factor 6 regulates tumor cell invasion through the activation of the MEK/ERK signaling pathway. Proc. Natl. Acad. Sci. USA *101*, 9671–9676.

Takeichi, M. (1991). Cadherin cell adhesion receptors as a morphogenetic regulator. Science *251*, 1451–1455.

Totaro, A., Paris, S., Asperti, C., and de Curtis, I. (2007). Identification of an intramolecular interaction important for the regulation of GIT1 functions. Mol. Biol. Cell *18*, 5124–5138.

Vestweber, D., and Kemler, R. (1985). Identification of a putative cell adhesion domain of uvomorulin. EMBO J. *4*, 3393–3398.

Zantek, N. D., Azimi, M., Fedor-Chaiken, M., Wang, B., Brackenbury, R., and Kinch, M. S. (1999). E-cadherin regulates the function of the EphA2 receptor tyrosine kinase. Cell Growth Differ. *10*, 629–638.

Zelinski, D. P., Zantek, N. D., Stewart, J. C., Irizarry, A. R., and Kinch, M. S. (2001). EphA2 overexpression causes tumorigenesis of mammary epithelial cells. Cancer Res. *61*, 2301–2306.

Zhang, H., Webb, D. J., Asmussen, H., and Horwitz, A. F. (2003). Synapse formation is regulated by the signaling adaptor GIT1. J. Cell Biol. *161*, 131–142.

THE JOURNAL OF BIOLOGICAL CHEMISTRY VOL. 284, NO. 13, pp. 8548–8556, March 27, 2009

FBP17 Mediates a Common Molecular Step in the Formation of Podosomes and Phagocytic Cups in Macrophages*[S]

Received for publication, July 23, 2008, and in revised form, December 29, 2008 Published, JBC Papers in Press, January 20, 2009, DOI 10.1074/jbc.M805638200

Shigeru Tsuboi[‡1], Hidetoshi Takada[§], Toshiro Hara[§], Naoki Mochizuki[¶], Tomihisa Funyu[‖], Hisao Saitoh[‖], Yuriko Terayama[‖], Kanemitsu Yamaya[‖], Chikara Ohyama[**], Shigeaki Nonoyama[‡‡], and Hans D. Ochs[§§]

From the [‡]Infectious and Inflammatory Disease Center, Burnham Institute for Medical Research, La Jolla, California 92037, the [§]Department of Pediatrics, Graduate School of Medical Sciences, Kyushu University, Fukuoka 812-8582, Japan, the [¶]Department of Structural Analysis, National Cardiovascular Center Research Institute, Osaka 565-8565, Japan, the [‖]Oyokyo Kidney Research Institute, Hirosaki 036-8243, Japan, the [**]Department of Urology, Hirosaki University School of Medicine, Hirosaki 036-8562, Japan, the [‡‡]Department of Pediatrics, National Defense Medical College, Saitama 359-0042, Japan, and the [§§]Department of Pediatrics, Research Center for Immunity and Immunotherapy, Seattle Children's Hospital Research Institute, Seattle, Washington 98101

Macrophages act to protect the body against inflammation and infection by engaging in chemotaxis and phagocytosis. In chemotaxis, macrophages use an actin-based membrane structure, the podosome, to migrate to inflamed tissues. In phagocytosis, macrophages form another type of actin-based membrane structure, the phagocytic cup, to ingest foreign materials such as bacteria. The formation of these membrane structures is severely affected in macrophages from patients with Wiskott-Aldrich syndrome (WAS), an X chromosome-linked immunodeficiency disorder. WAS patients lack WAS protein (WASP), suggesting that WASP is required for the formation of podosomes and phagocytic cups. Here we have demonstrated that formin-binding protein 17 (FBP17) recruits WASP, WASP-interacting protein (WIP), and dynamin-2 to the plasma membrane and that this recruitment is necessary for the formation of podosomes and phagocytic cups. The N-terminal EFC (extended FER-CIP4 homology)/F-BAR (FER-CIP4 homology and Bin-amphiphysin-Rvs) domain of FBP17 was previously shown to have membrane binding and deformation activities. Our results suggest that FBP17 facilitates membrane deformation and actin polymerization to occur simultaneously at the same membrane sites, which mediates a common molecular step in the formation of podosomes and phagocytic cups. These results provide a potential mechanism underlying the recurrent infections in WAS patients.

Podosomes (see Fig. 1*A*) are micron-scale, dynamic, actin-based protrusions observed in motile cells such as macrophages, dendritic cells, osteoclasts, certain transformed fibroblasts, and carcinoma cells (1). Podosomes play an important role in macrophage chemotactic migration, which is critical for recruitment of leukocytes to inflamed tissues. Podosomes are both adhesion structures and the sites of extracellular matrix degradation (2). Adhesion to and degradation of the extracellular matrix are essential processes for the successful migration of macrophages in tissues. Podosomes occur in most macrophages and can be observed by differentiating human primary monocytes into macrophages with macrophage-colony stimulating factor-1 (M-CSF-1)[2] and staining the F-actin using phalloidin (3, 4). Podosomes labeled in this way appear as F-actin-rich dots (see Fig. 1*C*). Podosome formation has recently been directly observed *in vitro* and *in vivo* in leukocyte migration through the endothelium, diapedesis (5).

Phagocytosis of bacterial pathogens is one of the most important primary host defense mechanisms against infections. The phagocytic cup (see Fig. 1*B*) is an actin-based membrane structure formed at the plasma membrane of phagocytes, including macrophages, upon stimulation with foreign materials such as bacteria. The phagocytic cup captures and ingests foreign materials, and its formation is an essential first step in phagocytosis leading to the digestion of foreign materials (6, 7). When macrophages are stimulated by foreign materials, podosomes disappear, and phagocytic cups, which are also rich in F-actin, are formed to ingest the foreign materials (see Fig. 1*D*).

Wiskott-Aldrich syndrome (WAS) is an X chromosome-linked immunodeficiency disorder. Patients with WAS suffer from severe bleeding, eczema, recurrent infection, autoimmune diseases, and an increased risk of lymphoreticular malignancy (8–10). The causative gene underlying WAS encodes Wiskott-Aldrich syndrome protein (WASP) (11). WASP deficiency due to the mutation or deletion causes defects in adhesion, chemotaxis, phagocytosis, and the development of hematopoietic cells in WAS patients (10).

* This work was supported, in whole or in part, by National Institutes of Health Grant R01HD042752 (to S. T.). The costs of publication of this article were defrayed in part by the payment of page charges. This article must therefore be hereby marked "*advertisement*" in accordance with 18 U.S.C. Section 1734 solely to indicate this fact.

[S] The on-line version of this article (available at http://www.jbc.org) contains six supplemental figures.

[1] To whom correspondence should be addressed: Dept. of Biochemistry, Oyokyo Kidney Research Institute, 90 Yamazaki, Kozawa, Hirosaki 036-8243, Japan. Tel.: 81-172-87-1221; Fax: 81-172-87-1228; E-mail: tsuboi@oyokyo.jp.

[2] The abbreviations used are: M-CSF-1, macrophage-colony stimulating factor-1; FBP17, formin-binding protein 17; WAS, Wiskott-Aldrich syndrome; WASP, Wiskott-Aldrich syndrome protein; N-WASP, neuronal WASP; WIP, WASP interacting-protein; EFC domain, extended FER-CIP4 homology domain; F-BAR domain, FER-CIP4 homology and Bin-amphiphysin-Rvs domain; PMA, phorbol 12-myristate 13-acetate; GFP, green fluorescence protein; siRNA, short interfering RNA; FITC, fluorescein isothiocyanate; PDZ-GEF, PDZ-guanine nucleotide exchange factor; HEK293 cells, human embryonic kidney 293 cells; HA, hemagglutinin; SH3, src homology 3 domain; dSH3, SH3 domain deletion; GST, glutathione *S*-transferase; , $PI(4,5)P_2$, phosphatidylinositol 4,5-bisphosphate; siFBP, siRNA for FBP17; siC, scrambled control siRNA.

The formation of podosomes and phagocytic cups is severely affected in macrophages from WAS patients (3, 12, 42), suggesting that WASP is involved in the formation of these structures. However, the detailed molecular mechanisms of their formation remain unknown. WASP is complexed with a cellular WASP-interacting partner, WASP-interacting protein (WIP) (13, 14). Recently, two groups (including us) have demonstrated that WASP and WIP form a complex and that the WASP-WIP complex is required for the formation of podosomes (4, 15) and phagocytic cups (16). Here, we identified formin-binding protein 17 (FBP17) as a protein interacting with the WASP-WIP complex and examined the role of FBP17 in the formation of podosomes and phagocytic cups.

EXPERIMENTAL PROCEDURES

Reagents and Antibodies—Recombinant human macrophage-colony stimulating factor-1 (M-CSF-1) was purchased from R&D Systems (Minneapolis, MN). Phenylmethylsulfonyl fluoride, leupeptin, pepstain A, aprotinin, IGEPAL CA-630, paraformaldehyde, saponin, bovine serum albumin, 3-methyladenine, latex beads (3 μm in diameter), phorbol 12-myristate 13-acetate (PMA), human IgG, glycerol, Triton X-100, anti-FLAG monoclonal antibody (M2), and anti-β-actin antibody were purchased from Sigma-Aldrich. The anti-WASP monoclonal antibody, anti-WIP polyclonal antibody, and anti-Myc monoclonal antibody (9E10) were obtained from Santa Cruz Biotechnology Inc. (Santa Cruz, CA). The anti-dynamin-2 antibody was purchased from BD Biosciences. The rat anti-hemagglutinin (HA) monoclonal antibody (3F10) was purchased from Boehringer Ingelheim (Ridgefield, CT). The Cy2-labeled anti-rat IgG was obtained from Jackson ImmunoResearch Laboratories (West Grove, PA).

Yeast Two-hybrid Screening—We screened a human lymphocyte cDNA library (Origene Technology Inc., Rockville, MD) using a full-length WIP as bait. A cDNA encoding full-length WIP was cloned into pGilda (BD Biosciences Clontech). The EGY48 yeast strain was transformed with pGilda-WIP, the human lymphocyte cDNA library, and pSH18–34, a reporter plasmid for the β-galactosidase assay. Transformants were assayed for Leu prototrophy, and a filter assay was performed for β-galactosidase measurement (17).

Cells and Transfection—THP-1 and human embryonic kidney (HEK) 293 cells were purchased from the American Type Culture Collection (Manassas, VA) and cultured in RPMI1640 and Dulbecco's modified Eagle's high glucose medium (Invitrogen), respectively, both supplemented with 10% fetal bovine serum. For human primary monocyte isolation, 10–30 ml of peripheral blood was drawn from healthy volunteers and WAS patients after informed consent was obtained. Monocytes were prepared from peripheral blood samples (10–30 ml) using a monocyte isolation kit II (Miltenyi Biotech Inc., Auburn, CA). Transfection of THP-1 cells and monocytes was performed with a Nucleofector device using a cell line Nucleofector kit V and a human monocyte Nucleofector kit, respectively, according to the manufacturer's instructions (Amaxa Biosystems, Gaithersburg, MD). Transfection of HEK293 cells was performed using SuperFect transfection reagent (Qiagen, Valencia, CA). THP-1 cells and monocytes were co-transfected with the FBP17 constructs and a GFP-expressing plasmid, pmaxGFP (Amaxa Biosystems Inc.), as a transfection marker. The transfection efficiency measured using pmaxGFP was 40–50% for THP-1 cells and 10–20% for monocytes.

RNA Interference—A short interfering RNA (siRNA) for FBP17 and its scrambled control siRNA was synthesized by Dharmacon (Lafayette, CO). The targeting sequence was 5′-CCCACTTCATATGTCGAAGTCTGTT-3′ (18). THP-1 cells and monocytes were transfected with siRNA using a cell line Nucleofector kit V and a human monocyte Nucleofector kit, respectively, and a Nucleofector device. Cells were co-transfected with an fluorescein isothiocyanate (FITC)-conjugated control siRNA, BLOCK-IT (Invitrogen), as a transfection marker. The transfection efficiency measured using BLOCK-IT was 40–50% for THP-1 cells and 10–20% for monocytes.

Immunoprecipitation—For immunoprecipitation of WASP from THP-1 cells, 2×10^7 cells were lysed in buffer A (50 mM Tris-HCl, pH 7.5, 75 mM NaCl, 1% Triton X-100, 1 mM phenylmethylsulfonyl fluoride, 1 μg/ml leupeptin, 1 μg/ml pepstatin A, 1 μg/ml aprotinin). Lysates were centrifuged at 10,000 $\times$ *g* at 4 °C for 15 min. The supernatant was incubated with 2 μg/ml anti-WASP monoclonal antibody (Santa Cruz Biotechnology) at 4 °C for 2 h and then incubated with anti-mouse IgG agarose (Sigma). The resin binding the immune complex was washed three times with 0.5 ml of buffer B (50 mM Tris-HCl, pH 7.5, 10% glycerol, 0.1% Triton X-100), and the complex was eluted with 1× Laemmli's SDS-PAGE sample buffer. Eluted proteins were subjected to SDS-PAGE and analyzed by immunoblotting for WASP, WIP, and FBP17.

GST Pull-down Assay—Glutathione *S*-transferase (GST) and a fusion protein of GST and the src homology 3 (SH3) domain of FBP17 (548–609 amino acids) (GST-FSH3) were purified from *Escherichia coli* (XL-1B) extracts using glutathione-Sepharose-4B. HEK293 cells were transfected with the cDNAs of Myc- or FLAG-tagged protein and lysed in buffer A. Lysates from the transfected cells were incubated with the affinity matrices of GST alone or GST-FSH3 at 4 °C for 1 h. After a 1-h incubation, the matrices were washed five times with buffer A, and pull-down samples were analyzed by immunoblotting using anti-Myc or anti-FLAG antibody.

Immunofluorescence Microscopy—THP-1 cells and monocytes grown on coverslips were differentiated into macrophages by incubation with 12.5 ng/ml PMA (Sigma) and 20 ng/ml M-CSF-1 (R&D Systems), respectively, for 72 h. HEK293 cells were transfected with various cDNA constructs and then cultured on coverslips for 48 h. Cells were fixed with 4% (w/v) paraformaldehyde, permeabilized with 0.1% (w/v) saponin, and blocked with 1% (w/v) bovine serum albumin. Cells were stained with primary antibodies and Alexa Fluor 488- or Alexa Fluor 564-labeled secondary antibodies (Invitrogen). Cells were also stained with Alexa Fluor 568-labeled phalloidin (Invitrogen). Cell staining was examined under a fluorescence microscope (Zeiss Axioplan AR) or an MRC 1024 SP laser point scanning confocal microscope (Bio-Rad).

Assays for the Formation of Podosomes and Phagocytic Cups—The formation of podosomes and phagocytic cups was assayed by visualizing these actin-based membrane structures by F-actin staining as described previously (4, 16). Briefly, podosomes

in differentiated THP-1 cells or macrophages were visualized by F-actin staining with Alexa Fluor 568-phalloidin. To form phagocytic cups in differentiated THP-1 cells or macrophages, latex beads (3 μm, Sigma) were opsonized with 0.5 mg/ml human IgG (Sigma), and cells grown on coverslips were incubated with the IgG-opsonized latex beads at 37 °C for 10 min in the presence of 10 mM 3-methyladenine (Sigma) to stabilize the phagocytic cups (16). The phagocytic cups were then also visualized with Alexa Fluor 568-phalloidin. Cells were examined under a fluorescence microscope (Zeiss Axioplan AR).

Assays for Macrophage Migration and Phagocytosis—For the macrophage migration assay, human macrophages (2×10^5 cells) were plated onto chemotaxis membranes with 5-μm pores (Corning, Acton, MA) coated with 0.15% gelatin/phosphate-buffered saline placed within Boyden chamber inserts. M-CSF-1 was used as a chemoattractant and diluted in serum-containing RPMI 1640 medium in lower chambers. After a 4-h incubation, non-migrating cells were removed by gently wiping the upper surface of the filter. The filter was removed from the inserts using a razor blade and mounted onto glass plates, and the number of migrating cells was counted under a fluorescence microscope. For the phagocytosis assay, human macrophages (1×10^6 cells) were seeded on coverslips and incubated with 0.5 ml of RPMI 1640 medium containing IgG-opsonized latex beads (3 μm) at 4 °C for 10 min, allowing the beads to attach to cells. Phagocytosis was initiated by adding 1.5 ml of preheated RPMI 1640 medium, and the cells were incubated with the beads at 37 °C for 30 min. Control plates were incubated at 4 °C to estimate nonspecific binding of latex beads to the cells. After incubation, the cells were vigorously washed with phosphate-buffered saline, and the number of intracellular latex beads was determined by counting beads within cells under a fluorescence microscope. The percentage of phagocytosis was calculated as the total number of cells with at least one bead as a percentage of the total number of cells counted. At least 100 cells were examined.

Cell Fractionation—To prepare the cytoplasmic and membrane fractions, macrophages (1×10^6 cells) were washed with ice-cold phosphate-buffered saline and suspended in 50 mM Tris-HCl buffer, pH 7.5, containing 1 mM EDTA and proteinase inhibitors as described above. The cell suspensions were sonicated four times on ice for 5 s each using a bath-type sonicator followed by ultracentrifugation at 265,000 × *g* at 4 °C for 2 h. The supernatant was used as the cytosolic fraction, and the pellet was resuspended in 50 mM Tris-HCl, pH 7.5, containing 1 mM EDTA and used as the membrane fraction. Anti-Caspase-3 (Santa Cruz Biotechnology) and anti-sodium potassium ATPase antibodies (AbCam, Inc., Cambridge, MA) were used to determine the purity of the cytosolic and membrane fractions, respectively.

Statistics—Statistically significant differences were determined using the Student's *t* test. Differences were considered significant if $p < 0.05$.

RESULTS

FBP17 Binds to the WASP-WIP Complex and Dynamin-2 in Macrophages—To explore the detailed molecular mechanisms of the formation of podosomes and phagocytic cups, we searched for a protein interacting with the WASP-WIP complex. We identified FBP17 as a WIP-binding protein in a yeast two-hybrid screen using the full-length WIP as bait. FBP17 was originally identified as a protein binding to formin, a protein that regulates the actin cytoskeleton (19). FBP17 is a member of the *Schizosaccharomyces pombe* Cdc15 homology (PCH) protein family (20) and contains an N-terminal extended FER-CIP4 homology (EFC) domain (also known as the FER-CIP4 homology and Bin-amphiphysin-Rvs (F-BAR) domain), protein kinase C-related kinase homology region 1 (HR1), and an SH3 domain (Fig. 1*E*). The EFC/F-BAR domain has membrane binding and deformation activities, and FBP17 is involved in endocytosis in transfected COS-7 cells (18, 21, 22).

To confirm that FBP17 directly interacts with WIP or WASP, we performed GST pull-down assays using a fusion protein of GST and the SH3 domain of FBP17 (GST-FBPSH3). Purified GST and the GST-FSH3 fusion protein were subjected to SDS-PAGE (Fig. 1*F*, *lanes 1* and *2*). The HEK293 transfected cells express the Myc- and FLAG-tagged proteins (Fig. 1*F*, *lanes 3–6*). The results from the GST pull-down assays were shown (Fig. 1*F*, *lanes 7–14*). Both WASP and WIP were pulled down by GST-FSH3 (Fig. 1, *lanes 10* and *14*), indicating that the SH3 domain of FBP17 directly interacts with both proteins.

It has previously been shown that FBP17 binds to N-WASP and dynamin in transfected cells (18, 21). We examined whether FBP17 binds to WASP, WIP, and dynamin-2 in macrophages. THP-1 (human monocyte cell line) cells closely resemble monocyte-derived macrophages when differentiated by stimulation with PMA (23) and form podosomes and phagocytic cups that are morphologically and functionally indistinguishable from those in primary macrophages (supplemental Fig. 1) (4, 16, 23). WASP was immunoprecipitated from the lysates of PMA-differentiated THP-1 cells with an anti-WASP monoclonal antibody (Fig. 1*G*, *lanes 2*, *5*, and *8*) followed by immunoblotting using antibodies to FBP17 (21), WASP, and WIP. Both WIP and FBP17 co-immunoprecipitated with WASP (Fig. 1*G*, *lanes 5* and *8*). FBP17 also co-immunoprecipitated with dynamin-2 (Fig. 1*G*, *lanes 14*). These results, taken together with the results in Fig. 1*F*, suggest that FBP17 binds to the WASP-WIP complex and dynamin-2 in macrophages.

We next used immunofluorescence to examine whether FBP17 localizes at podosomes and phagocytic cups because the WASP-WIP complex is an essential component of podosomes (4, 15) and phagocytic cups (16). THP-1 cells transfected with FLAG-tagged FBP17 (FLAG-FBP17) and differentiated by stimulation with PMA were stained with an anti-FLAG monoclonal antibody to visualize FBP17 and with phalloidin to visualize the F-actin in podosomes and phagocytic cups (Fig. 1, *H* and *I*, *left* and *middle panels*). Merged images revealed that both F-actin and FBP17 are present in podosomes and phagocytic cups (Fig. 1, *H* and *I*, *right panels*), indicating that FBP17 localizes at podosomes and phagocytic cups.

Importance of FBP17 in the Formation of Podosomes and Phagocytic Cups—To determine the importance of FBP17 in the formation of podosomes and phagocytic cups, we knocked down FBP17 in THP-1 cells with siRNAs. To confirm that the expression of FBP17 was knocked down in cells, we transfected THP-1 cells with siRNAs, prepared lysates from the total

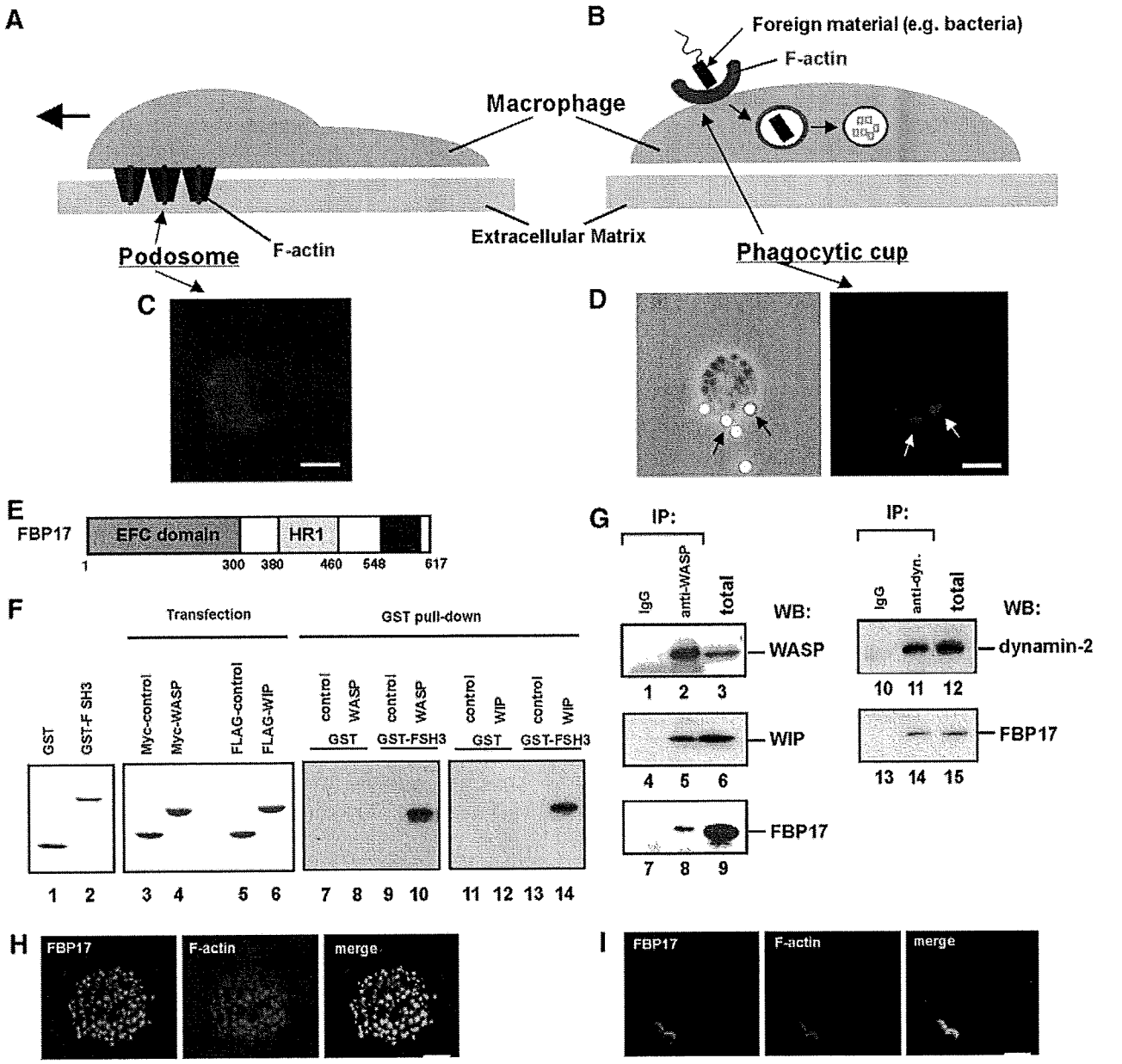

FIGURE 1. **FBP17 is a component of podosomes and phagocytic cups.** *A* and *B*, schematic drawings of podosomes (*A*) and a phagocytic cup (*B*) in macrophages. *C*, podosomes in macrophages were visualized by F-actin staining using Alexa Fluor 568-phalloidin. *D*, macrophages incubated with IgG-opsonized latex beads formed phagocytic cups to ingest the beads. A phase contrast image of a macrophage forming phagocytic cups (*left panel*). *Black arrows* indicate the latex beads ingested by the macrophage. Phagocytic cups were visualized by F-actin staining using Alexa Fluor 568-phalloidin (*right panel*). *White arrows* indicate the phagocytic cups. The *bar* is 10 μm. *E*, the domain organization of FBP17. *HR1*, protein kinase C-related kinase homology region 1. *F*, FBP17 interacts directly with WASP and WIP via its SH3 domain. GST and the GST-FBP17 SH3 domain fusion protein (GST-FSH3) were purified from bacteria extracts. Purified proteins were subjected to SDS-PAGE and stained with Coomassie Brilliant Blue (*lanes 1* and *2*). HEK293 cells were transfected with the cDNAs of Myc-tagged control protein (Myc-PDZ-GEF), Myc-WASP, FLAG-PDZ-GEF, or FLAG-WIP, and the expression of those proteins were analyzed by immunoblotting (*lanes 3–6*). Lysates from the HEK293 transfected cells were incubated with the affinity matrices of GST alone or GST-FSH3. Pull-down samples were analyzed by immunoblotting using anti-Myc antibody (*lanes 7–10*) and anti-FLAG antibody (*lanes 11–14*). *G*, FBP17 binds WASP, WIP, and dynamin-2. WASP was immunoprecipitated (*IP*) from the lysates of PMA-differentiated THP-1 cells with anti-WASP or a control IgG (*left panel, lanes 1–9*). The WASP immunoprecipitates and total lysates were analyzed by immunoblotting (*WB*) for WASP (*lanes 1–3*), WIP (*lanes 4–6*), and FBP17 (*lanes 7–9*). Dynamin was also immunoprecipitated from the THP-1 cell lysates with an anti-dynamin polyclonal antibody. The dynamin immunoprecipitates and total lysates were analyzed by immunoblotting for dynamin-2 (*lanes 10–12*) and FBP17 (*lanes 13–15*). *H* and *I*, confocal laser scanning micrographs of PMA-differentiated THP-1 cells. *H*, THP-1 cells transfected with FLAG-tagged FBP17 cDNA (FBP17) were double-stained with an anti-FLAG monoclonal antibody (*left panel*) and phalloidin (*center panel*) to visualize the F-actin in podosomes. *Yellow* indicates co-localization of FBP17 (*green*) and F-actin, podosomes (*red*) (*right panel*). *I*, THP-1 cells transfected with FLAG-FBP17 cDNA were incubated with IgG-opsonized latex beads and double-stained with anti-FLAG antibody and phalloidin. Phagocytic cups were visualized by F-actin staining (*center panel*). *Yellow* indicates co-localization of FBP17 (*green*) and F-actin, phagocytic cups (*red*) (*right panel*). The *bar* is 10 μm.

siRNAs-transfected cells, and analyzed the expression level of FBP17 by immunoblotting. THP-1 cells transfected with the siRNA for FBP17 expressed ~40% less FBP17 than cells transfected with a scrambled control siRNA based on the immunoblots (Fig. 2*A*, *lanes 1* and *2*) but expressed the same level of β-actin (Fig. 2*A*, *lanes 3* and *4*). The transfection efficiency of